

EFFECTS OF THERMOPHYSICAL PROPERTIES ON HEAT TRANSFER AT THE INTERFACE OF TWO IMMISCIBLE FLUIDS IN A VERTICAL DUCT: NUMERICAL STUDY**J.C. Umavathi^{1*} and O. Anwar Bég²**¹*Visiting Professor, Dipartimento di Ingegneria, Università degli Studi della Campania "Luigi Vanvitelli", Via Roma 29, 81031, Aversa (CE), Italy.*²*Professor of Engineering Science & Director Multi-Physical Engineering Sciences Group (MPESG), Department of Aeronautical/Mechanical Engineering, School of Science, Engineering and Environment (SEE), University of Salford, Manchester, M5 4WT, UK.****Corresponding author- email: drumavathi@rediffmail.com****ABSTRACT**

A comprehensive theoretical and numerical investigation is presented for two fluids with different physical properties. The effects of buoyancy and viscous heating are addressed. Non-isothermal wall conditions are applied at the walls. The front and rear walls of the duct are perfectly insulated. Numerical solutions for the reduced non-dimensional Navier-Stokes equations and coupled energy conservation equation are obtained using a finite difference method with second-order accuracy. Opting suitable conditions at the interface the two different solutions for two different fluids are extracted. The effects of Grashof number (thermal buoyancy parameter), viscosity ratio, thermal conductivity ratio, Eckert number (dissipation parameter), Prandtl number and duct aspect ratios (for the two immiscible fluid regions) on the flow field are visualized graphically. The value of the average Nusselt number is also tabulated for the two-fluid model. A grid-independence study is conducted. The solutions obtained by the numerical code are also validated by comparing with the benchmark solutions of the one fluid model and also with the simpler solutions of two fluid models available in the literature. Promoting Grashof number, Eckert number, Prandtl number and upper region aspect ratio (i.e. simultaneous decrease lower region aspect ratio) the Nusselt number increases at the left wall and decreases at the right wall in both the regions. However, the converse effect is computed with greater values of ratio of conductivity and viscosity. With increasing viscosity ratio parameter significant flow acceleration is induced in the upper half region of the duct whereas deceleration is caused at the bottom of the duct. Prescribing different values of aspect ratios in the upper and lower duct regions is found to generate a noticeable movement of the interface. The computations show that percentage changes in $Nu|_{y=0}$ (heat transfer rate at the left wall of the duct) are 19.3334, 19.9350, 19.9423, 19.9965, 20.1926% in correspondence with a change in Grashof number from 5, 10, 20, 50, to 100 respectively. Percentage changes in Nusselt number are 19.9102, 19.9547, 19.9999, 20.0451, 20.0901% for values of Prandtl number of 0.01, 0.5, 1.0, 1.5, 2 respectively. The simulations are relevant to crystal growth technologies, buoyancy-driven fires in atria and geophysical convection.

KEYWORDS: *Immiscible fluids; thermal convection; buoyancy; aspect ratio; variable thermophysical properties; interface; viscous dissipation; finite difference method; Nusselt number; 3-D rectangular duct.*

NOMENCLATURE

$A^{(i)}$ aspect ratio in region-1 $\left(\frac{a^{(i)}}{2b} \right)$

$a^{(i)}$	height of the duct
b	horizontal distance of the duct
C_p	constant pressure at specific heat
Ec	Eckert number $\left(\frac{\overline{W}^{(1)2}}{C_p (T^{(w2)} - T^{(w1)})} \right)$
Gr	Grashof number $\left(\frac{g \rho^{(1)2} \beta^{(1)} b^3 (T^{(w2)} - T^{(w1)})}{\mu^{(1)2}} \right)$
$K^{(i)}$	thermal conductivity
m	ratio of thermal expansion co-efficient $\left(\frac{\beta_t^{(2)}}{\beta_t^{(1)}} \right)$
$Nx^{(i)}, Ny$	number of grids
n	ratio of densities $\left(\frac{\rho^{(2)}}{\rho^{(1)}} \right)$
P	pressure
p	gradient of pressure $\left(\frac{b^2}{\mu^{(1)} \overline{W}^{(1)}} \frac{\partial P}{\partial Z} \right)$
Pr	Prandtl number $\left(\frac{\mu^{(1)} C_p}{K^{(1)}} \right)$
Re	Reynolds number $\left(\frac{\rho^{(1)} b \overline{W}^{(1)}}{\mu^{(1)}} \right)$
$T^{(i)}$	temperature
$T^{(wi)}$	wall temperature
$\overline{W}^{(i)}$	average velocity
$W^{(i)}$	velocity
$\Delta x^{(i)}$ and Δy	step lengths in the x and y directions
$X^{(i)}, Y, Z$	space co-ordinates

Greek Symbols

α	viscosity ratio $\left(\frac{\mu^{(1)}}{\mu^{(2)}}\right)$
$\beta_t^{(i)}$	thermal expansion coefficient
β	conductivity ratio $\left(\frac{K^{(2)}}{K^{(1)}}\right)$
$\mu^{(i)}$	viscosity

Superscripts

$i=1,2$ quantities for region-1 and region-2 respectively.

1. INTRODUCTION

Natural convection in open-ended cavities has received considerable attention among applied mathematicians and engineering scientists by numerical and experimental approach. This interest evolves owing to the usefulness of duct geometries in architectural solar heating (Moosavi *et al.*, 2014), enclosure fire dynamics (Zukoski *et al.* 1980), electronic cooling component, geothermal movement and aircraft habitation (Davis, 1968, Kimura and Bejan, 1984, Hall *et al.*, 1988). The primitive flow structure is to consider free convection for the fluid filled in a closed conduit applying non-isothermal conditions at the walls. Investigations of thermal properties in a rectangular duct for thermally insulated horizontal walls have been extensively documented in the scientific literature and culmination accuracy has been observed between experimental and the solutions obtained using numerical methods.

The examples of free convection in tubes can be observed in crystal growth and heat storage systems. The increased speed of modern computers and improvements in numerical algorithms have greatly accelerated activity in computational simulations of natural convection in enclosure ducts. Many different numerical methodologies have been employed to analyze a variety of thermal convection transport phenomena in rectangular duct systems. Rudraiah *et al.* (1995) studied free convection in the existence

of magnetic field in a conduit. A numerical study was described by Umavathi *et al.* (2005) for convective flow in a vertical channel employing the Brinkman-Forchheimer-extended Darcy equation. Hydromagnetic mixed convection flow with asymmetric and asymmetric wall heat conditions and heat source/sink was investigated by Ali (2002), who showed that flow reversal occurs *only for asymmetric* wall temperatures and is enhanced with heat source (generation) and applied magnetic field. Volume-average equations were developed by Ali (2013) for the hydrodynamic mixed convection non-Darcian flow with or without heat sources embedded in a porous matrix, and backflow zones were identified. Using temperature-dependent properties Ali (2001) formulated the problems of unsteady laminar fully developed flow and heat transfer with source/sink for an electrically conducting fluid. Turbulent and laminar convective flow in a chamber using finite volume of conducting solid component was analyzed by Marcelo (2005) applying a finite volume computational algorithm to compare two different approaches (i.e. the *porous-continuum*, *homogeneous* or *macroscopic* and the *continuum*, *heterogeneous* or *microscopic models*). A multi-step differential transform method was implemented to solve the nonlinear differential equations in third grade fluid flow by Keimanesh *et al.* (2011), who demonstrated that this method is significantly faster and easier to implement than homotopy methods. Kefavati *et al.* (2011) used the D2Q9 grid and Bhatnagar-Gross-Krook (BGK) model for relaxation to equilibrium in Lattice Boltzmann method (LBM) computations of free convection of silicon dioxide-water nanofluids in narrow enclosures with aspect ratios ranging from 0.5 to 2 and for Rayleigh numbers between 1000 and 100,000. Bhargava *et al.* (2017) deployed a variational finite element code and implicit finite difference method to study the double-diffusive convection of micropolar fluids in rectangular cavities. Fully developed free convection of a micropolar fluid in a vertical channel was considered by Ali *et al.* (2002), who showed that increasing non-Newtonian (micropolar) effects decelerate the flow. Zehba and Raiza (2016) utilized an incompressible smoothed particle hydrodynamics (ISPH) method to study copper-oxide water nanofluid natural convection in multiple enclosure geometries. Venkatadri *et al.* (2020) employed the Harlow-Welch marker-and-cell (MAC) difference scheme to compute hydromagnetic phase-change natural convection in variable aspect ratio enclosures. Ravnik *et al.* (2008) simulated natural convection in

cubic and parallelepipedal inclined enclosures with a boundary element method (BEM) with aspect ratio of 1:2. Kuharat *et al.* (2019) used a finite volume SIMPLE algorithm to simulate buoyancy effects on natural convection flows of gold-water nanofluid in three-dimensional prismatic enclosures, considering inclination, aspect ratio and volume fraction effects. Ali *et al.* (2018) reviewed the applications of nanofluids in micro channels. They concluded that the Nusselt number was escalated with Reynolds number. The presence of nano particles augments thermal and fluid flow properties in microchannels. Convective flow, heat transfer and entropy generation in an odd-shaped geometry was presented by Salva and Chamkha (2014). They showed that the Rayleigh number elevates the Nusselt number and entropy generation heat transfer term and suppresses the entropy generation viscous term. Using convective boundary conditions RamReddy *et al.* (2013) studied the influence of Soret (thermo-diffusive) effect on nanofluid flow in the boundary layer region. They concluded that the Soret effect boosts the skin friction, heat, nanoparticle mass and regular mass transfer rates in the medium. Hybrid $Al_2O_3 - Cu$ water nanofluid free convection in a differentially heated porous cavity by Mehryan *et al.* (2017) The presence of heat source and the impact of its location on natural convection in a C-shaped enclosure saturated by a nanofluid was investigated by Rushal *et al.* (2017). They found that with heat source located in the upper part and with high Rayleigh numbers, there was an increase in Nusselt number. Other studies include Abu-Nada (2015) (which featured a dissipative particle dynamics numerical code for a differentially heated cavity), Bég *et al.* (2016) (who used network electrothermal simulation and forward time centered space FTCS difference schemes for natural convection-radiation flows in annular duct solar enclosures) and Pepper and Wang (2008) who applied an optimized hp-adaptive finite element model for partitioned duct enclosures.

The majority of the above investigation were confined to closed zones occupied by only one fluid. Many problems relating to industrial materials processing, petrophysics of reservoirs, atmospheric stratified flows and fire dynamics (air and smoke interface) involve *multi-fluid* dynamics. The behavior of different fluid layers is also of considerable interest in the design and operation of fluid experiments in low gravity space environments in modern spacelab astronautics (Ostrach, 1982). Longlois (1985)

and Schwabe (1986) claim that for good quality crystal growth, the natural convection in non-miscible fluids are more relevant. Considering the model of hexadecane and water, Sparrow *et al.* (1986) elucidated the transport characteristics in two-fluid enclosure convection. The combination of spindle oil-water and spindle oil-ethylene glycol filled in a conduit was explored by Kimura *et al.* (1986). Parallel numerical computations were also conducted by Kimura *et al.* (1986). These studies furnished important data for evaluating the mechanisms dominating natural convection in two-layered liquid systems. Unsteady flow of a particulate suspension in an electrically conducting fluid through channels and circular pipes was examined by Ali (2000). Ali and Mansour (2009) focused on the modeling of the problem of hydrodynamic buoyancy-induced flow of a particulate suspension through a vertical pipe with source/sink effects. Prakash and Koster (1996, 1997) present the excellent surveys of key works focused on not miscible fluids.

To recognize the structure and physics of two non-miscible fluids, several studies have been executed which speculate that there exist two specific mechanisms which explain the linking between the thermal and mechanical forces. In non-isothermal scenarios, a variety of complicated circumstances arise. To perceive in a proper way the conditions *at the interface* needs careful explanation with mathematical models. The added dynamical increments are the stresses at the interface and change in the shape at the interface. Meyer and Garder (1954) were the first to analyze the logistics for the interface that occur between the fluid and porous matrix. A key study for forced convection occurring in multiple non-immiscible fluids was presented by Kuznetsov (2000). Assuming that the shear stresses are equal at the interface Vafai and Kim (1990) determined exact solutions. Various types of conditions at the interface were summarized by Alzami and Vafai (2001). A three-layer model for the flow through a porous matrix with different permeabilities and thermal conductivities was developed by Nield and Kuznetsov (2000). Fully developed laminar free convection flow in a vertical channel filled with two immiscible fluids (i.e. micropolar fluid and viscous Newtonian fluid) was examined by Prathap Kumar *et al.* (2010). They observed that greater rheological (micropolar) material parameter suppresses velocity whereas it enhances the microrotation (angular velocity) in both the regions. Hydromagnetic two-phase flow in a

channel was investigated by Ali (1995), who established that the flow rates of the fluid and particle phases were reduced in the presence of particles in the channel. The flow of dusty and electrically conducting fluid through a pipe was considered by Ali (1994) who showed that volumetric flow rates and skin friction coefficient are reduced with stronger magnetic field. Packham and Shail (1971), Shail (1973) and Loharsbi and Sahai (1998) have all scrutinized the interfacial conditions that appear between two non-miscible fluids. The best model for non-Darcy flows is that which assumes stresses and velocities to be continuous at the clear and porous matrix interface. This robust approach has been implemented extensively by Umavathi and co-workers (1997, 2001, 2005, 2006a,b, 2007) who have analyzed the fluid mechanics of diverse combinations of non-miscible fluids. Betchancourt *et al.* (1999) studied natural convection of a two-layer fluid in a side-heated cavity. They did not make any priori assumptions on the shape and dynamical role of the interface. The behavior of the interface was established as part of the solution. Unsteady oscillatory flow in a horizontal composite porous medium was simulated by Umavathi *et al.* (2001). They concluded that the oscillation amplitude amplifies the flow field. Kim and Sin (2006) experimented on two-phase flow distribution of air-water annular flow in a parallel flow heat exchanger.

Inspite of the emphasis on the appearance of convection in non-miscible fluids, significant questions in this area of thermal science still remain unanswered. This is the motivation for the present communication which considers in detail the thermal convection in immiscible viscous two-fluid layered natural convection *with variable thermophysical properties* in a vertical tube. A second-order accurate finite difference method is implemented to solve the non-dimensional conservation equations with appropriate boundary and interface conditions. Extensive visualization of computations is provided for a range of Grashof number (thermal buoyancy parameter), viscosity ratio, thermal conductivity ratio, Eckert number (dissipation parameter), Prandtl number and duct aspect ratios (for the two immiscible fluid regions). Verification of the finite difference code is achieved via comparisons with a range of benchmark solutions for the one-fluid model and two-fluid models available in the literature. A novelty of the present work is therefore the specific appraisal of variable thermophysical properties on immiscible thermal convection duct (tube) flow. Previous studies have been largely

confined to constant property models and have generally neglected viscous heating effects also.

2. PHYSICAL MODEL AND ASSUMPTIONS

Figure 1 illustrates the physical model and adopted co-ordinate system. The vertical rectangular conduit is filled with two immiscible viscous fluids with different properties. The flow is assumed to be steady, laminar and hydrodynamically fully-developed i.e., only the Z -component W of the fluid is non-vanishing. $\frac{(a^{(1)} + a^{(2)})}{2}$ is the length and b is the width of the tube. Non-isothermal wall conditions are enforced ($T^{(w1)}$ at $Y=0$ and $T^{(w2)}$ at $Y=b$, where $T^{(w2)} > T^{(w1)}$). The front and rear sides of the tube are insulated, i.e. $\frac{\partial T^{(1)}}{\partial X^{(1)}} = 0$ at $X^{(1)} = 0$ and $\frac{\partial T^{(2)}}{\partial X^{(2)}} = 0$ at $X^{(2)} = \frac{(a^{(1)} + a^{(2)})}{2}$. The region $0 \leq X^{(1)} \leq \frac{a^{(1)}}{2}$ and $0 \leq Y \leq b$ is occupied by a viscous, incompressible fluid of density $\rho^{(1)}$, viscosity $\mu^{(1)}$, thermal expansion coefficient $\beta_t^{(1)}$ and thermal conductivity $K^{(1)}$. The region $\frac{a^{(1)}}{2} \leq X^{(2)} \leq \frac{a^{(2)}}{2}$ and $0 \leq Y \leq b$ is occupied by a different (immiscible) fluid having density $\rho^{(2)}$, viscosity $\mu^{(2)}$, thermal expansion coefficient $\beta_t^{(2)}$ and thermal conductivity $K^{(2)}$. Both fluids are assumed to be Newtonian and have constant properties except the density variation in the buoyancy term of the momentum equation which is approximated with the Oberbeck-Boussinesq approximation. Under these assumptions, the governing equations for momentum and energy conservation in the two regions of the duct are:

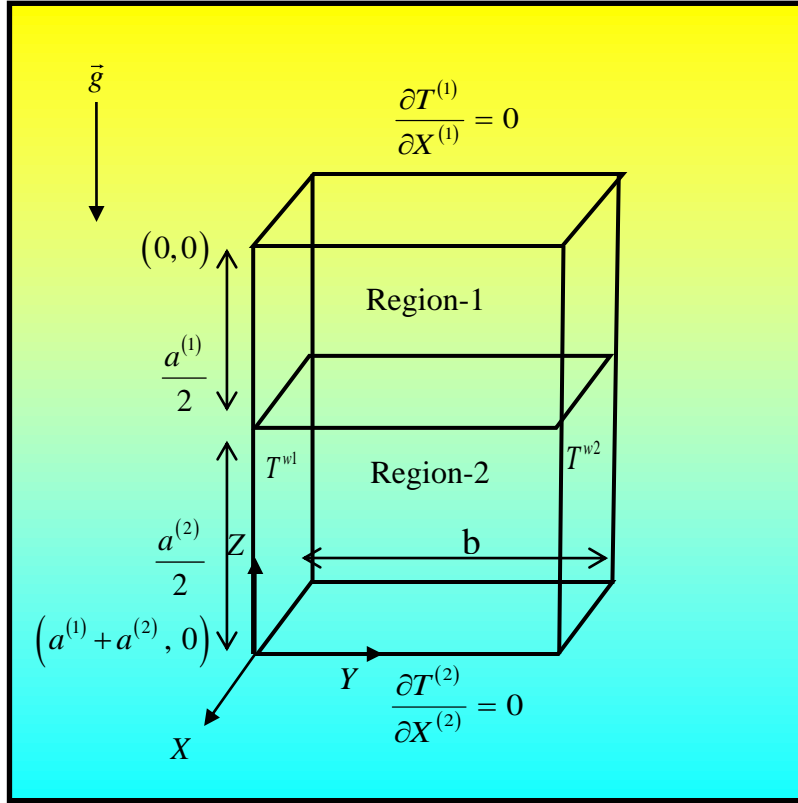


Figure 1 Physical configuration for two-fluid natural convection in a 3-dimensional rectangular duct

Region-1 (upper zone)

$$\frac{\partial^2 W^{(1)}}{\partial X^{(1)2}} + \frac{\partial^2 W^{(1)}}{\partial Y^2} + \frac{\rho^{(1)} \bar{g} \beta^{(1)} (T^{(1)} - T_0)}{\mu^{(1)}} = \frac{\partial P}{\partial Z} \quad (1)$$

$$\frac{\partial^2 T^{(1)}}{\partial X^{(1)2}} + \frac{\partial^2 T^{(1)}}{\partial Y^2} + \frac{\mu^{(1)}}{K^{(1)}} \left[\left(\frac{\partial W^{(1)}}{\partial X^{(1)}} \right)^2 + \left(\frac{\partial W^{(1)}}{\partial Y} \right)^2 \right] = 0 \quad (2)$$

Region-2 (lower zone)

$$\frac{\partial^2 W^{(2)}}{\partial X^{(2)2}} + \frac{\partial^2 W^{(2)}}{\partial Y^2} + \frac{\rho^{(2)} \bar{g} \beta^{(2)} (T^{(2)} - T_0)}{\mu^{(2)}} = \frac{\partial P^{(2)}}{\partial Z} \quad (3)$$

$$\frac{\partial^2 T^{(2)}}{\partial X^{(2)2}} + \frac{\partial^2 T^{(2)}}{\partial Y^2} + \frac{\mu^{(2)}}{K^{(2)}} \left[\left(\frac{\partial W^{(2)}}{\partial X^{(2)}} \right)^2 + \left(\frac{\partial W^{(2)}}{\partial Y} \right)^2 \right] = 0 \quad (4)$$

where $W^{(1)}$ and $W^{(2)}$ are the velocities of the fluids in region-1 and region-2, $T^{(1)}$ and $T^{(2)}$ are the temperatures of the fluids in region-1 and region-2, $\rho^{(1)}$ and $\rho^{(2)}$ are the densities of the fluids in region-1 and region-2, $\mu^{(1)}$ and $\mu^{(2)}$ are the viscosities of the fluids in region-1 and region-2, $K^{(1)}$ and $K^{(2)}$ are the thermal conductivities of the fluid in region-1 and region-2, \vec{g} is the acceleration due to gravity, T_0 is the reference temperature, and $X^{(1)}, X^{(2)}, Y$ are the space co-ordinates. We assume that

$$T_0 = \frac{(T^{(w1)} + T^{(w2)})}{2}. \quad \text{The no slip condition requires that the velocity must vanish at the}$$

boundaries. The gradient of temperature $(T^{(w2)} - T^{(w1)})$ and gradient of pressure causes for the convection in the tube. Further, the velocity, temperature, shear stress and flux are continuous at the region of interface (following Alzami and Vafai, 2001). Eqns. (1) to (4) are solved subject to the following boundary and interface conditions:

$$\begin{aligned} W^{(1)} = 0, \quad T^{(1)} = T^{w1} & \quad \text{at } Y = 0 \quad \text{for } 0 \leq X_1 < \frac{a^{(1)}}{2} \\ W^{(1)} = 0, \quad T^{(1)} = T^{w2} & \quad \text{at } Y = b \quad \text{for } 0 \leq X^{(1)} < \frac{a^{(1)}}{2} \\ W^{(1)} = 0, \quad \frac{\partial T^{(1)}}{\partial X^{(1)}} = 0 & \quad \text{at } X^{(1)} = 0 \quad \text{for } 0 \leq Y \leq b \\ W^{(1)} = W^{(2)}, \quad \mu^{(1)} \frac{\partial W^{(1)}}{\partial X^{(1)}} = \mu^{(2)} \frac{\partial W^{(2)}}{\partial X^{(2)}} & \quad \text{at } X = \frac{a^{(1)}}{2} \quad \text{for } 0 \leq Y \leq b \\ T^{(1)} = T^{(2)}, \quad K^{(1)} \frac{\partial T^{(1)}}{\partial X^{(1)}} = K^{(2)} \frac{\partial T^{(2)}}{\partial X^{(2)}} & \quad \text{at } X = \frac{a^{(1)}}{2} \quad \text{for } 0 \leq Y \leq b \\ W^{(2)} = 0, \quad T^{(2)} = T^{w1} & \quad \text{at } Y = 0 \quad \text{for } \frac{a^{(1)}}{2} < X^{(2)} \leq \frac{a^{(2)}}{2} \\ W^{(2)} = 0, \quad T^{(2)} = T^{w2} & \quad \text{at } Y = 0 \quad \text{for } \frac{a^{(1)}}{2} < X^{(2)} \leq \frac{a^{(2)}}{2} \\ W^{(2)} = 0, \quad \frac{\partial T^{(2)}}{\partial X^{(2)}} = 0 & \quad \text{at } X^{(2)} = \frac{a^{(1)} + a^{(2)}}{2} \quad \text{for } 0 \leq Y \leq b \end{aligned} \quad (5)$$

Introducing the following dimensionless variables:

$$x^{(1)} = \frac{X^{(1)}}{b}, \quad x^{(2)} = \frac{X^{(2)}}{b}, \quad y = \frac{Y}{b}, \quad w^{(1)} = \frac{W^{(1)}}{W^{(1)}}, \quad w^{(2)} = \frac{W^{(2)}}{W^{(2)}},$$

$$\theta^{(1)} = \frac{T^{(1)} - T^{(0)}}{T^{(w2)} - T^{(w1)}}, \quad \theta^{(2)} = \frac{T^{(2)} - T^{(0)}}{T^{(w2)} - T^{(w1)}} \quad (6)$$

Eqns. (1) to (4) can be written as:

Region-1

$$\frac{\partial^2 w^{(1)}}{\partial x^{(1)2}} + \frac{\partial^2 w^{(1)}}{\partial y^2} + \frac{Gr}{Re} \theta^{(1)} = p \quad (7)$$

$$\frac{\partial^2 \theta^{(1)}}{\partial x^{(1)2}} + \frac{\partial^2 \theta^{(1)}}{\partial y^2} + Pr Ec \left[\left(\frac{\partial w^{(1)}}{\partial x^{(1)}} \right)^2 + \left(\frac{\partial w^{(1)}}{\partial y} \right)^2 \right] = 0 \quad (8)$$

Region-2

$$\frac{\partial^2 w^{(2)}}{\partial x^{(2)2}} + \frac{\partial^2 w^{(2)}}{\partial y^2} + \frac{Gr \alpha n m}{Re} \theta^{(2)} = \alpha p \quad (9)$$

$$\frac{\partial^2 \theta^{(2)}}{\partial x^{(2)2}} + \frac{\partial^2 \theta^{(2)}}{\partial y^2} + \frac{Ec Pr}{\alpha \beta} \left[\left(\frac{\partial w^{(2)}}{\partial x^{(2)}} \right)^2 + \left(\frac{\partial w^{(2)}}{\partial y} \right)^2 \right] = 0 \quad (10)$$

The boundary and interface conditions given in Eqn. (5) using Eqn. (6) become:

$$w^{(1)} = 0, \quad \theta^{(1)} = -\frac{1}{2} \quad \text{at } Y=0 \quad \text{for } 0 \leq x^{(1)} < A^{(1)}$$

$$w^{(1)} = 0, \quad \theta^{(1)} = \frac{1}{2} \quad \text{at } Y=1 \quad \text{for } 0 \leq x^{(1)} < A^{(1)}$$

$$w^{(1)} = 0, \quad \frac{\partial \theta^{(1)}}{\partial x^{(1)}} = 0 \quad \text{at } x^{(1)} = 0 \quad \text{for } 0 \leq y \leq 1$$

$$w^{(1)} = w^{(2)}, \quad \frac{\partial w^{(1)}}{\partial x^{(1)}} = \frac{1}{\alpha} \frac{\partial w^{(2)}}{\partial x^{(2)}} \quad \text{at } x = A^{(1)} \quad \text{for } 0 \leq y \leq 1$$

$$\theta^{(1)} = \theta^{(2)}, \quad \frac{\partial \theta^{(1)}}{\partial x^{(1)}} = \beta \frac{\partial \theta^{(2)}}{\partial x^{(2)}} \quad \text{at } x = A^{(1)} \quad \text{for } 0 \leq Y \leq 1$$

$$w^{(2)} = 0, \quad \theta^{(2)} = -\frac{1}{2} \quad \text{at } y=0 \quad \text{for } A^{(1)} < x^{(2)} \leq A^{(2)}$$

$$\begin{aligned}
w^{(2)} = 0, \quad \theta^{(2)} = \frac{1}{2} & \quad \text{at } y=0 \quad \text{for } A^{(1)} < x^{(2)} \leq A^{(2)} \\
w^{(2)} = 0, \quad \frac{\partial \theta^{(2)}}{\partial x} = 0 & \quad \text{at } x = A^{(1)} + A^{(2)} \quad \text{for } 0 \leq y \leq 1
\end{aligned} \tag{11}$$

Here Gr is the Grashof number, Re is the Reynolds number, Ec is the Eckert number, Pr is the Prandtl number, m is the ratio of thermal expansion coefficients, n is the ratio of densities, α is the ratio of viscosities, β is the ratio of thermal conductivities, $A^{(1)}$ is the aspect ratio of region-1 and $A^{(2)}$ is the aspect ratio of region-2. These parameters are defined as follows:

$$\begin{aligned}
Gr = \frac{g \rho^{(1)2} \beta^{(1)} b^3 (T^{(w2)} - T^{(w1)})}{\mu^{(1)2}}, \quad Re = \frac{\rho^{(1)} b \bar{w}^{(1)}}{\mu^{(1)}}, \quad Ec = \frac{\bar{w}^{(1)2}}{C_p (T^{(w2)} - T^{(w1)})}, \quad P = \frac{b^2}{\mu^{(1)} \bar{w}^{(1)}} \frac{\partial P}{\partial Z} \\
Pr = \frac{\mu^{(1)} C_p}{K^{(1)}}, \quad m = \frac{\beta^{(2)}}{\beta^{(1)}}, \quad n = \frac{\rho^{(2)}}{\rho^{(1)}}, \quad \alpha = \frac{\mu^{(1)}}{\mu^{(2)}}, \quad \beta = \frac{K^{(2)}}{K^{(1)}}, \quad A^{(1)} = \frac{a^{(1)}}{2b}, \quad A^{(2)} = \frac{a^{(2)}}{2b}
\end{aligned} \tag{12}$$

3. NUMERICAL SOLUTION

Two layers of immiscible, viscous Boussinesq fluids are contained in the vertical rectangular duct. Since the governing equations are highly nonlinear, coupled, partial differential equations, extracting analytical solutions is intractable. Hence, a numerical solution is sought. Eqns. (7) – (10) are solved numerically under the boundary and interface conditions stipulated in Eqn. (11). The governing reduced steady Navier-Stokes equations, energy equation, slip condition, stress balance and kinetic condition at the free surface and the interface are all discretized using a robust finite difference method. The rectangular duct is divided into a grid of mesh points $(x_i^{(1)}, y_j)$ in region-1 and $(x_i^{(2)}, y_j)$ in region-2 where i ranges from 1 to $Nx1$ in region-1, i ranges from 1 to $Nx2$ in region-2 and j ranges from 1 to Ny in both the regions as shown in **Figure 2**. Δx and Δy represent the uniform step lengths in the x and y directions.

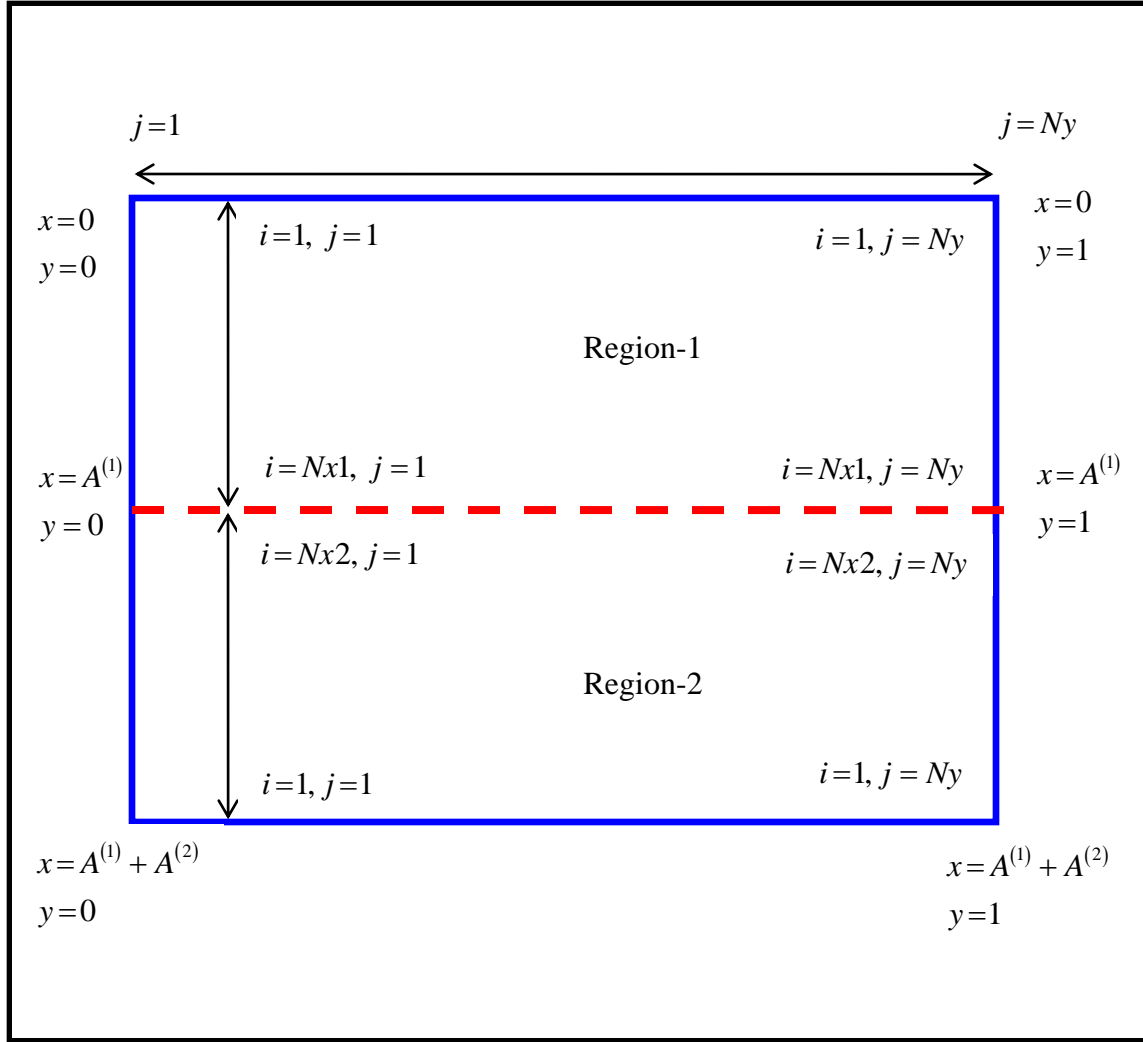


Figure 2 Grid points in numerical simulation

Space derivatives are discretized by means of a second-order central differencing scheme. Using central differences, Eqns. (7) – (10) at each grid point (i, j) take respectively the form of difference equations:

Region-1

$$\left(\frac{w_{i+1,j}^{(1)} - 2w_{i,j}^{(1)} + w_{i-1,j}^{(1)}}{(\Delta x^{(1)})^2} \right) + \left(\frac{w_{i,j+1}^{(1)} - 2w_{i,j}^{(1)} + w_{i,j-1}^{(1)}}{(\Delta y)^2} \right) + \frac{Gr}{Re} \theta_{i,j}^{(1)} - p = 0 \quad (13)$$

$$\left(\frac{\theta^{(1)}_{i+1,j} - 2\theta^{(1)}_{i,j} + \theta^{(1)}_{i-1,j}}{(\Delta x^{(1)})^2} \right) + \left(\frac{\theta^{(1)}_{i,j+1} - 2\theta^{(1)}_{i,j} + \theta^{(1)}_{i,j-1}}{(\Delta y)^2} \right) + \quad (14)$$

$$\Pr Ec \left[\left(\frac{w^{(1)}_{i+1,j} - w^{(1)}_{i-1,j}}{2\Delta x^{(1)}} \right)^2 + \left(\frac{w^{(1)}_{i,j+1} - w^{(1)}_{i,j-1}}{2\Delta y} \right)^2 \right] = 0$$

Region-2

$$\left(\frac{w^{(2)}_{i+1,j} - 2w^{(2)}_{i,j} + w^{(2)}_{i-1,j}}{(\Delta x^{(2)})^2} \right) + \left(\frac{w^{(2)}_{i,j+1} - 2w^{(2)}_{i,j} + w^{(2)}_{i,j-1}}{(\Delta y)^2} \right) + \frac{Gr \alpha nm}{Re} \theta^{(1)}_{i,j} - \alpha p^{(1)} = 0 \quad (15)$$

$$\left(\frac{\theta^{(2)}_{i+1,j} - 2\theta^{(2)}_{i,j} + \theta^{(2)}_{i-1,j}}{(\Delta x^{(2)})^2} \right) + \left(\frac{\theta^{(2)}_{i,j+1} - 2\theta^{(2)}_{i,j} + \theta^{(2)}_{i,j-1}}{(\Delta y)^2} \right) + \quad (16)$$

$$\frac{\Pr Ec}{\alpha \beta} \left[\left(\frac{w^{(2)}_{i+1,j} - w^{(2)}_{i-1,j}}{2\Delta x^{(2)}} \right)^2 + \left(\frac{w^{(2)}_{i,j+1} - w^{(2)}_{i,j-1}}{2\Delta y} \right)^2 \right] = 0$$

The interfacial and boundary conditions become:

$$\begin{aligned} w^{(1)}_{i,0} &= -w^{(1)}_{i,1}, & \theta^{(1)}_{i,0} &= -1 - \theta^{(1)}_{i,1}, & \text{at } Y=0 & \text{ for } 0 \leq x^{(1)} < A^{(1)} \\ w^{(1)}_{i,Ny+1} &= -w^{(1)}_{i,Ny}, & \theta^{(1)}_{i,Ny+1} &= 1 - \theta^{(1)}_{i,Ny}, & \text{at } Y=1 & \text{ for } 0 \leq x^{(1)} < A^{(1)} \\ w^{(1)}_{0,j} &= -w^{(1)}_{1,j}, & \theta^{(1)}_{1,j} &= \theta^{(1)}_{0,j}, & \text{at } x^{(1)}=0 & \text{ for } 0 \leq y \leq 1 \\ \left. \begin{aligned} w^{(2)}_{Nx2+1,j} &= w^{(1)}_{Nx+1,j} + w^{(1)}_{Nx1,j} - w^{(2)}_{Nx2,j}, \\ w^{(1)}_{Nx+1,j} &= \frac{\Delta x^{(1)}}{\alpha \Delta x^{(2)}} \left(w^{(2)}_{Nx2,j} - w^{(2)}_{Nx2+1,j} \right) + w^{(1)}_{Nx1,j}, \end{aligned} \right\} & \text{at } x = A^{(1)} & \text{ for } 0 \leq y \leq 1 \\ \left. \begin{aligned} \theta^{(2)}_{Nx2+1,j} &= \theta^{(1)}_{Nx+1,j} + \theta^{(1)}_{Nx1,j} - \theta^{(2)}_{Nx2,j}, \\ \theta^{(1)}_{Nx+1,j} &= \beta \frac{\Delta x^{(1)}}{\Delta x^{(2)}} \left(\theta^{(2)}_{Nx2,j} - \theta^{(2)}_{Nx2+1,j} \right) + \theta^{(1)}_{Nx1,j}, \end{aligned} \right\} & \text{at } x = A^{(1)} & \text{ for } 0 \leq Y \leq 1 \\ w^{(2)}_{i,0} &= -w^{(2)}_{i,1}, & \theta^{(2)}_{i,0} &= -1 - \theta^{(2)}_{i,1}, & \text{at } y=0 & \text{ for } A^{(1)} < x^{(2)} \leq A^{(2)} \\ w^{(2)}_{i,Ny+1} &= -w^{(2)}_{i,Ny}, & \theta^{(2)}_{i,Ny+1} &= 1 - \theta^{(2)}_{i,Ny}, & \text{at } y=0 & \text{ for } A^{(1)} < x^{(2)} \leq A^{(2)} \end{aligned}$$

$$w_{0,j}^{(2)} = -w_{1,j}^{(2)}, \quad \theta_{1,j}^{(2)} = \theta_{0,j}^{(2)} \quad \text{at } x = A^{(1)} + A^{(2)} \quad \text{for } 0 \leq y \leq 1 \quad (17)$$

The difference equations (13) – (16) are iterated after implementing the boundary conditions (17).

The nonlinear system is iteratively solved until two convergence criteria for velocity and temperature are satisfied. The iteration is stopped till value of the tolerance is achieved. The convergence criteria for both velocity and temperature is prescribed as 10^{-7} . Validation of the numerical code is achieved with both a grid independence study and by comparing with results from the available literature.

3.1. Grid-Independence Study

The average Nusselt number at the left wall of the tube is delineated in Table-1 for the autonomy of the grids. This table illustrates that refining the mesh density from 101×101 or 201×201 does not induce any *significant* modification in the solutions. Therefore mesh independence can be assumed to have been achieved with the 101×101 grid size and this grid design achieves acceptable accuracy.

Size of the grid	Average Nusselt number
11×11	1.00307968209008
51×51	1.00318803202941
101×101	1.00319174673160
151×151	1.00319243858460
201×201	1.00319268101602

Table-1 Grid independence study

3.2. Validation of the code by comparing with the available literature:

Validation of the present code is performed against three different studies from the available literature and the comparisons are shown in **Table-2**. Sanchez *et al.* (2004) and Kaminski and Prakash (1986) considered a cavity filled with single viscous fluid

and bounded by single or double walls with finite length and thermal conductivity whereas Oztop *et al.* (2009) considered the natural convection in a composite system (water-partition-air or air-partition-water) in a differentially heated square cavity. From **Table-2** one can conclude that the obtained results show good agreement with the literature, confirming the accuracy of the current finite difference numerical code.

Gr	β	Sanchez <i>et al.</i> (2004)	Kaminski and Prakash (1986)	Haken <i>et al.</i> (2009)	Present
10^5	5	2.078	2.08	2.187	2.10842848261764
10^5	25	3.49	3.42	3.394	3.48619977713609
10^6	5	2.80	2.87	2.741	2.80654437023274
10^6	25	5.91	5.89	5.815	5.90383813271836

Table-2 Comparison of the average Nusselt number with the literature

We further validate the code by comparing with benchmark solutions and with experimental results. Nikolay (2002) used a finite difference approximation to solve the Navier-Stokes equations under the Boussinesq-fluid assumption to analyse the flow and heat transfer in a two-layer system of an immiscible incompressible fluid in a rectangular enclosure. Computations were first performed for the widely used benchmark problem of a buoyancy-driven flow in a square cavity (de Vahl Davis, 1983; de Vahl Davis and Jones, 1983). The governing parameters in the present problem are *Grashof number*, *Reynolds number*, *Eckert number* and *Prandtl number*. In order to compare the results obtained with the benchmark solution the governing parameter required is the Rayleigh number. Since the Rayleigh number is the product of Grashof number and Prandtl number, the governing parameters are redefined to evaluate the average Nusselt number. **Table-3** displays the benchmark values and the values of Nikolay (2002). Nikolay (2002) also compared his computations with the laboratory experiment conducted by Dobretsov and Kyrdyashkin (1993). The experiment of Dobretsov and Kyrdyashkin (1993) consists of a two-layer model of mantle convection. Two immiscible liquids, glycerin and hexadecane were used in the experiment. Table-3 indicates that the

solutions obtained are in good agreement with the benchmark solutions and with the numerical solutions of Nikolay (2002), the latter also concurring with experimental data. This justifies confidence in the fact that the present finite difference numerical code produces acceptable results.

Rayleigh number	de Vahl Davis and Jones (1983)	Moshkin (2002)	Present
10^3	1.118	1.113	1.14350679110854
10^4	2.243	2.198	2.10739845012118
10^5	4.519	4.430	4.37982524603028
10^6	8.800	9.045	8.94901538324246

Table 3. Values of average Nusselt number

4. RESULTS AND DISCUSSION

A computational study has been performed to investigate natural convection in a vertical rectangular duct filled with two viscous immiscible fluids. The effects of governing parameters such as Grashof number Gr , viscosity ratio α , thermal conductivity ratio β , Eckert number Ec , Prandtl number Pr and aspect ratios $A^{(1)}$, $A^{(2)}$ on the flow field are evaluated numerically and visualized in Figs. 3 to 7. We note that all data has been carefully selected from standard sources in convective heat transfer, namely Gebhart *et al.* (1988), Kays and Crawford (1993), Rohsenow *et al.* (1998) and Pop and Ingham (2001). The data is physically representative of real fluids, geometries and actual thermophysical scenarios encountered in industrial heat duct systems.

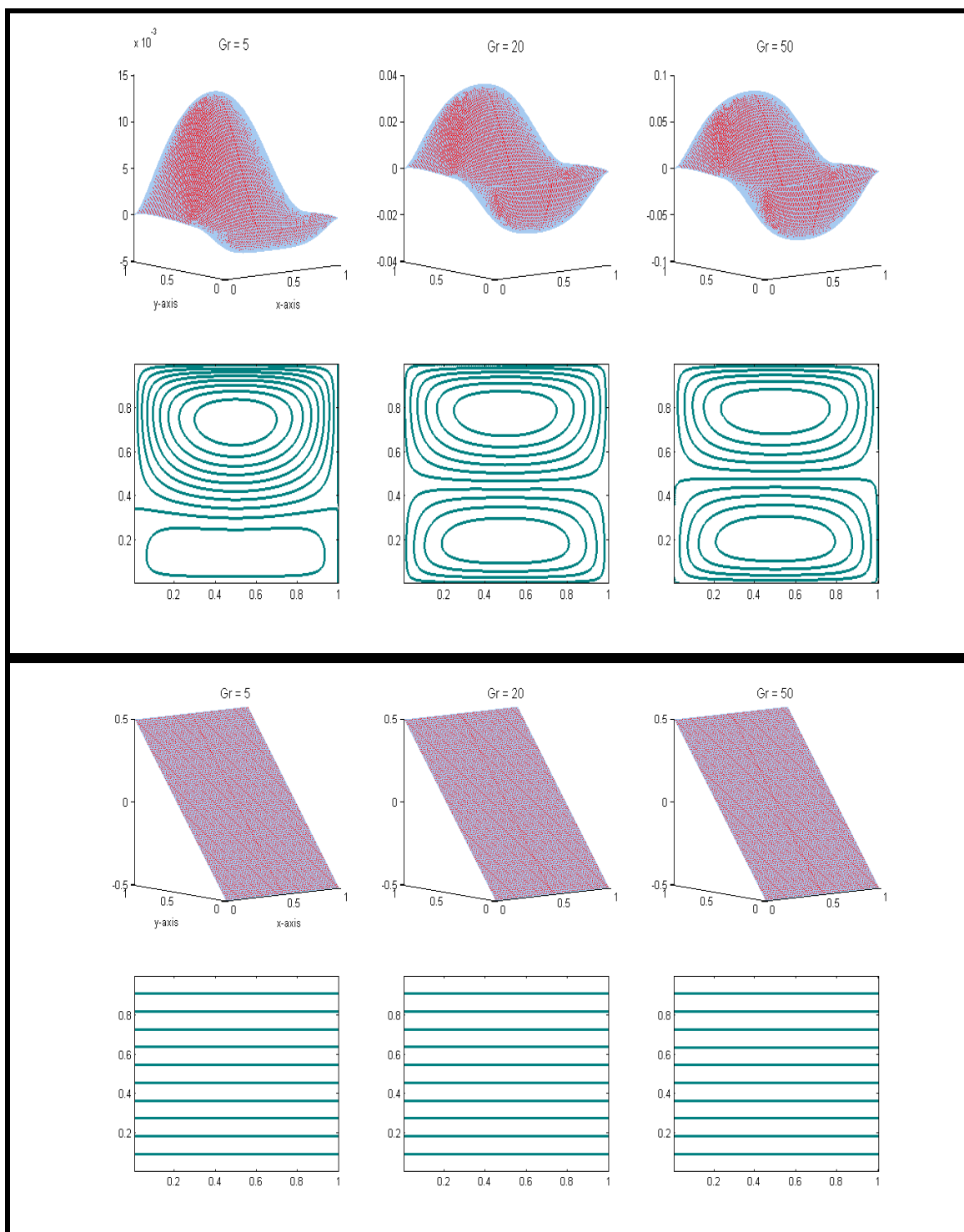


Figure 3a: Contours of the velocity and temperature distinct values of Grashof number, Gr

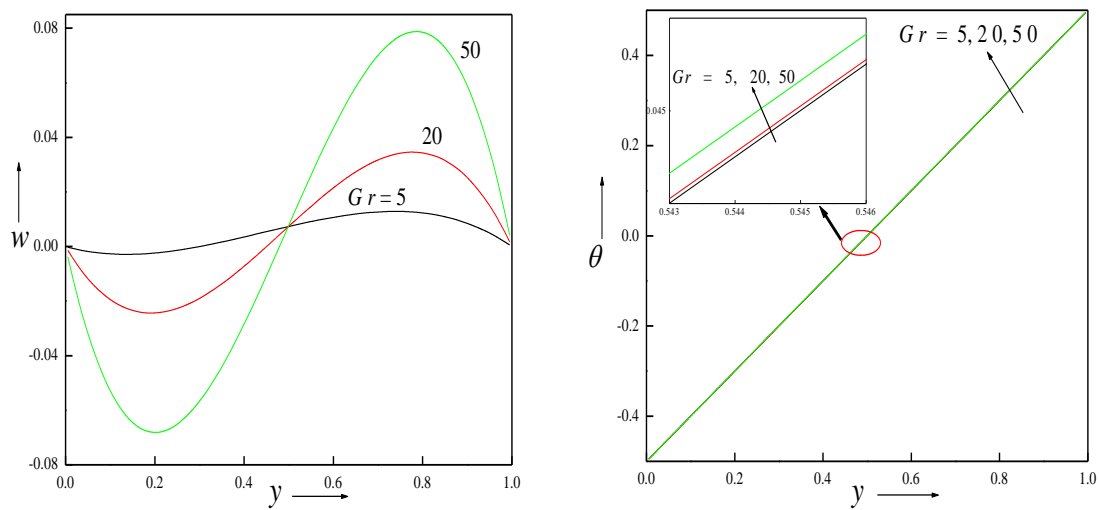
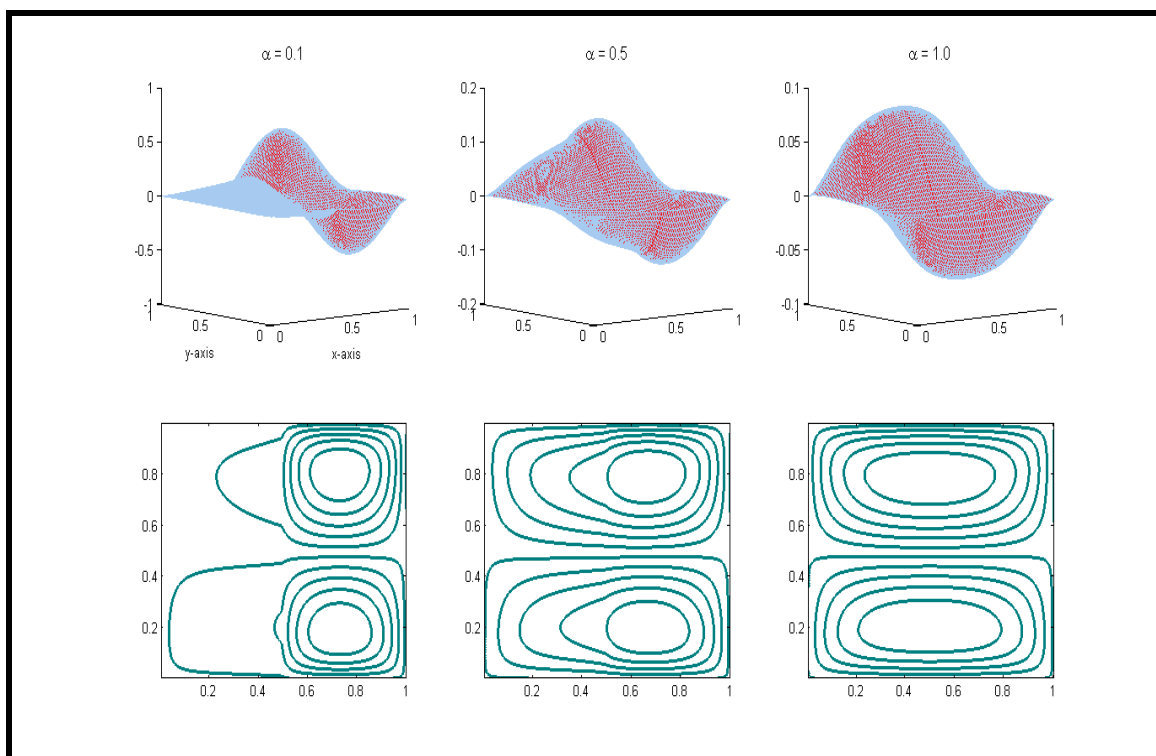


Figure 3b Portraits of velocity and temperature for different values of Grashof number, Gr



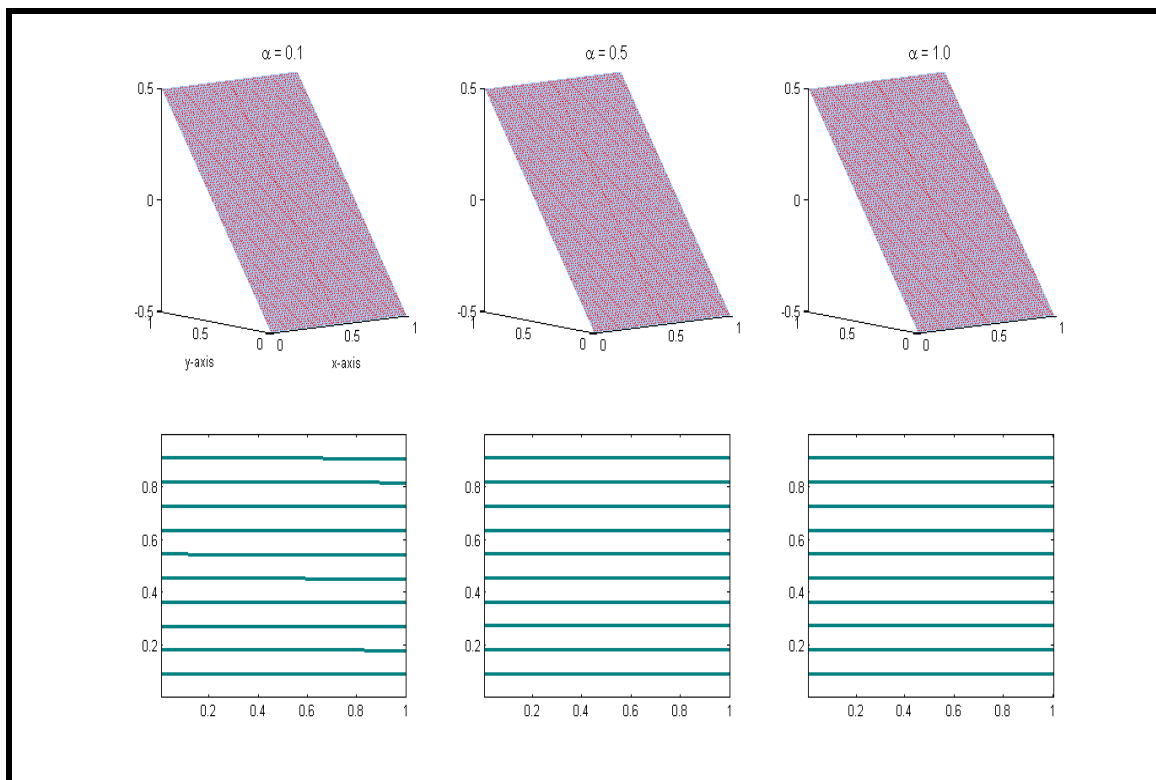


Figure 4a Contours of the velocity and temperature for distinct values of viscosity ratio, α

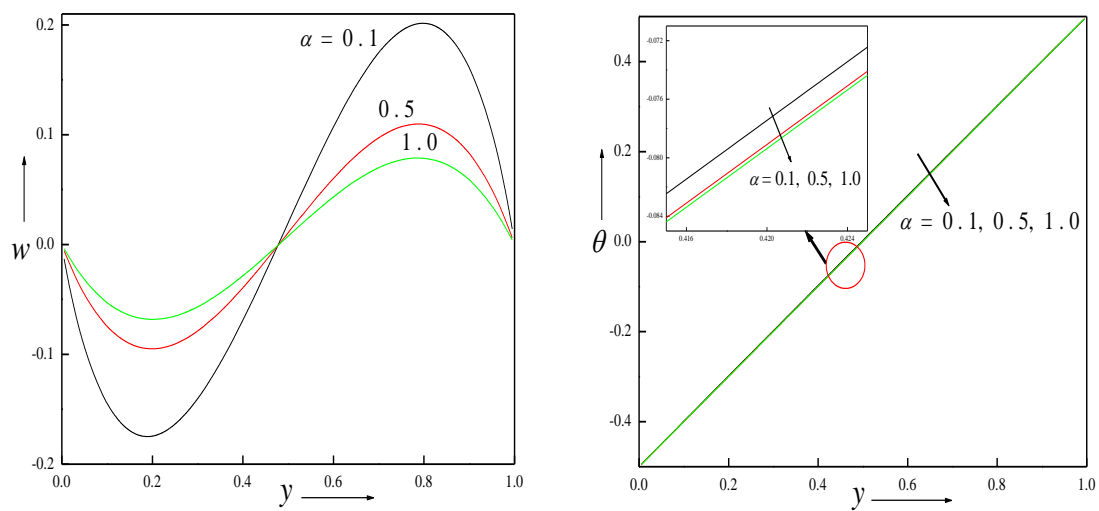


Figure 4b Portraits of velocity and temperature for different values of viscosity ratio, α

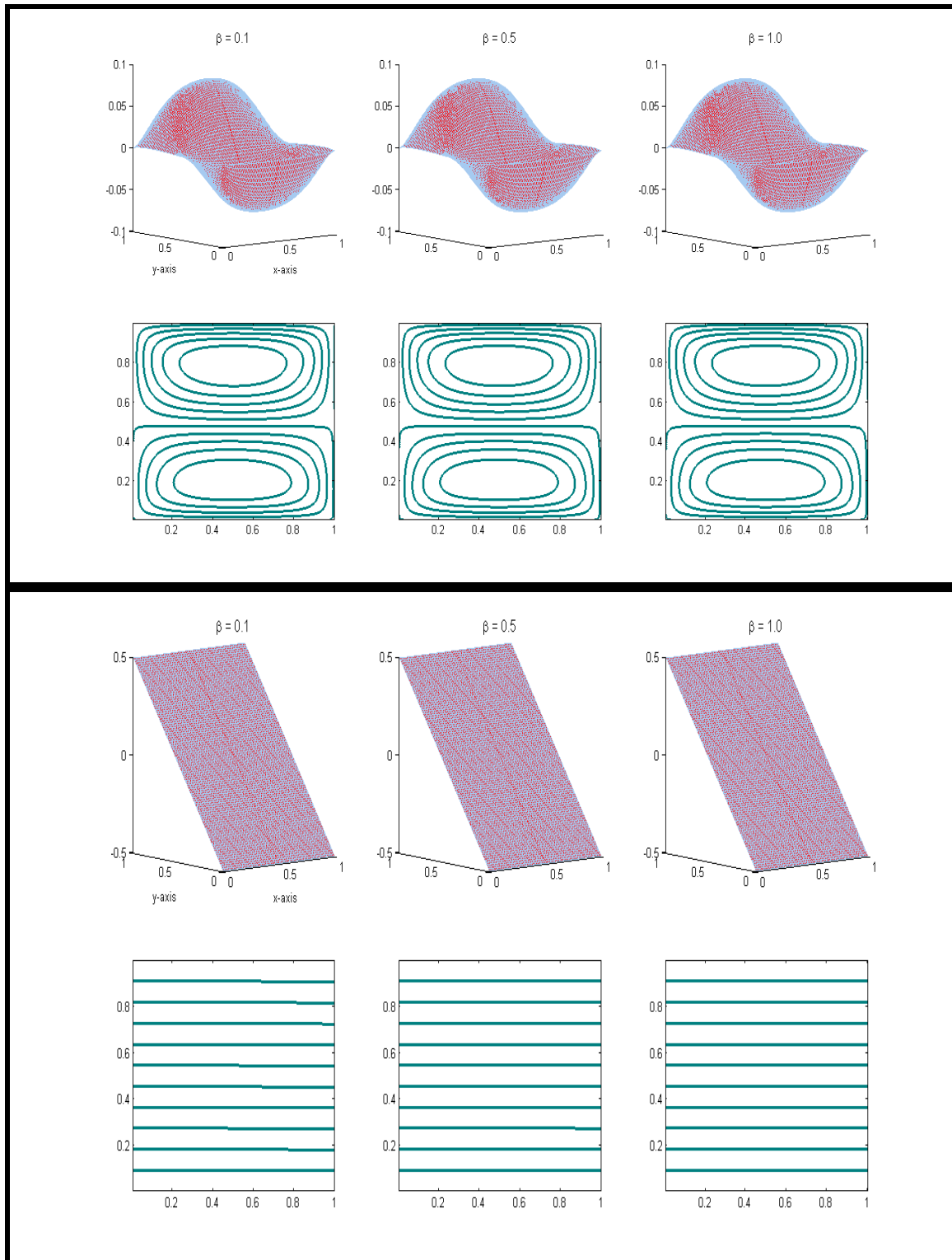


Figure 5a Contours of the velocity and temperature for distinct values of thermal conductivity ratio, β

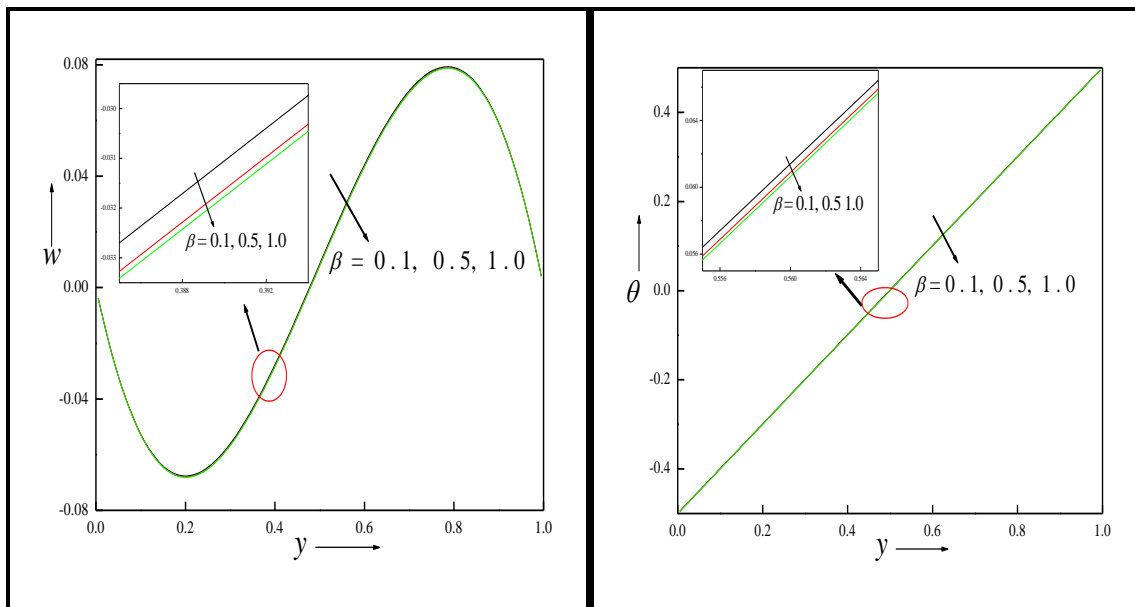
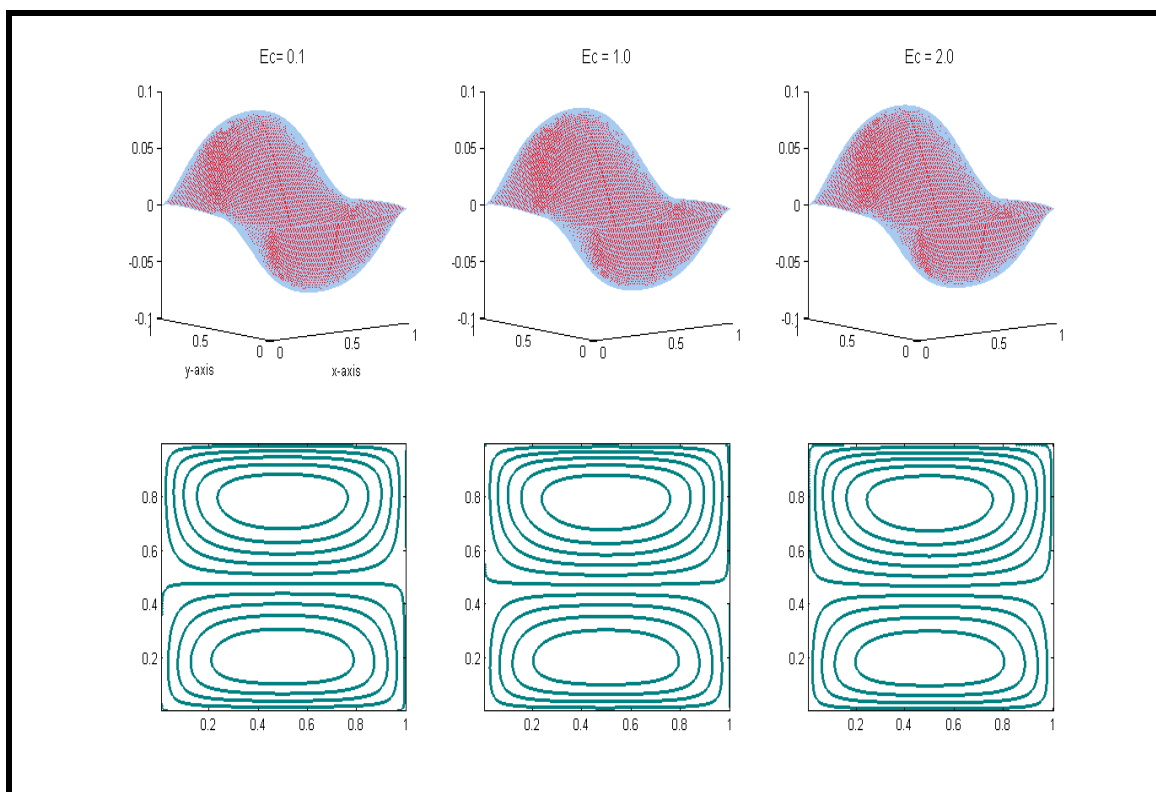


Figure 5b Portraits of velocity and temperature for different values of thermal conductivity ratio, β



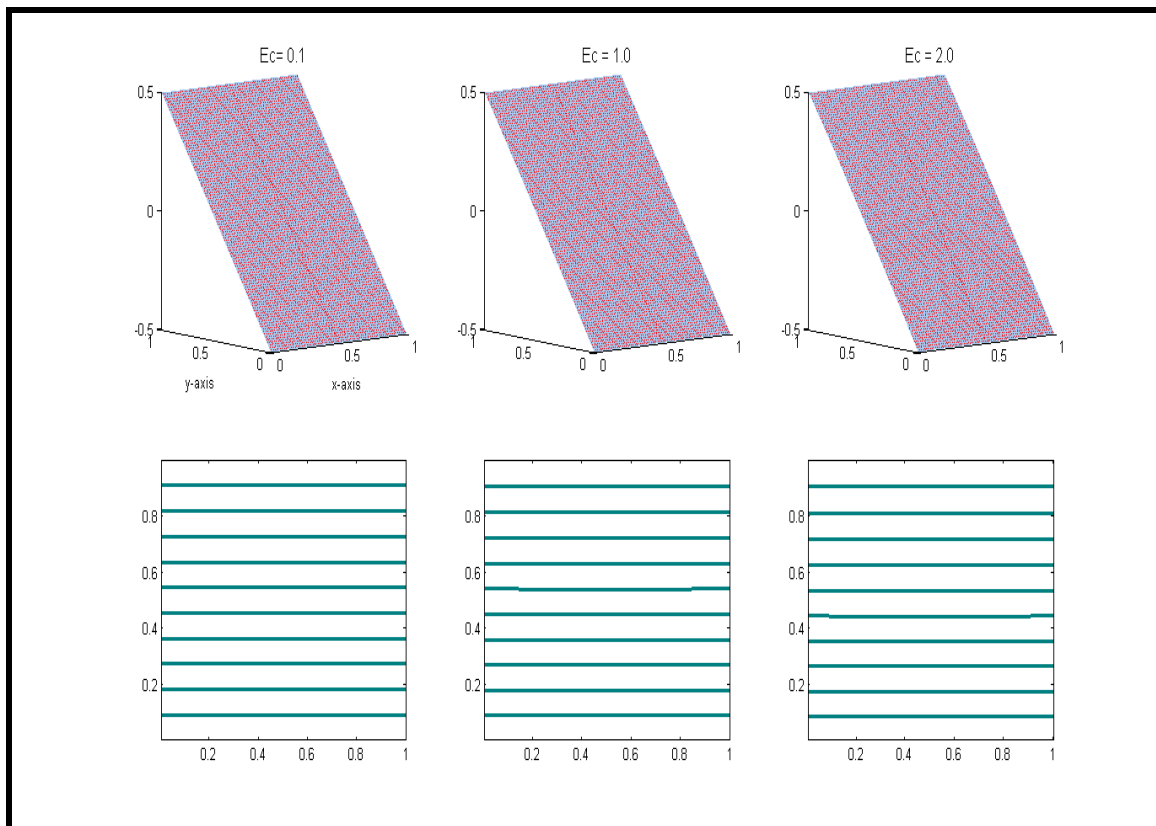


Figure 6a Contours of the velocity and temperature for distinct values of Eckert number, Ec

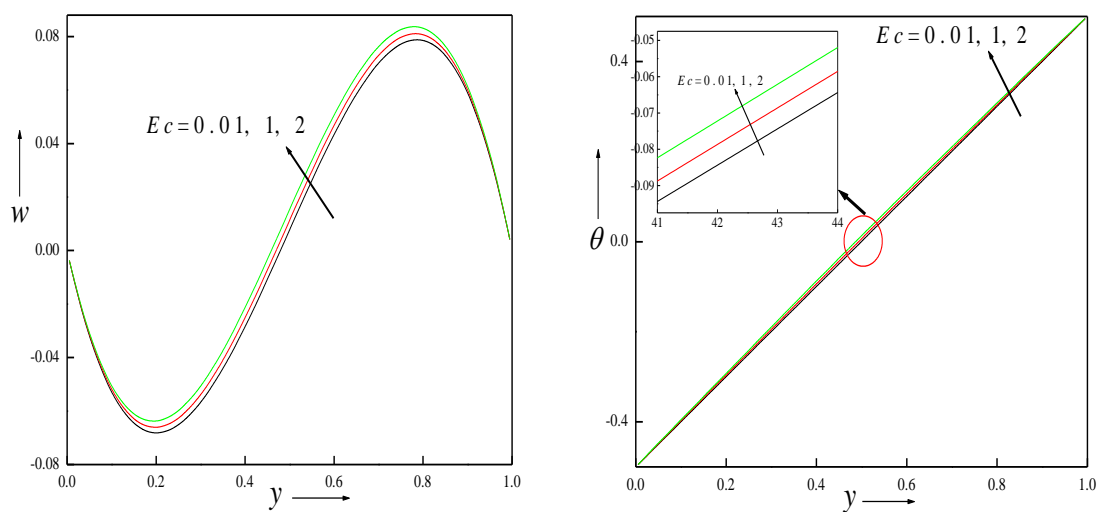


Figure 6b Portraits of velocity and temperature for different values of Eckert number, Ec

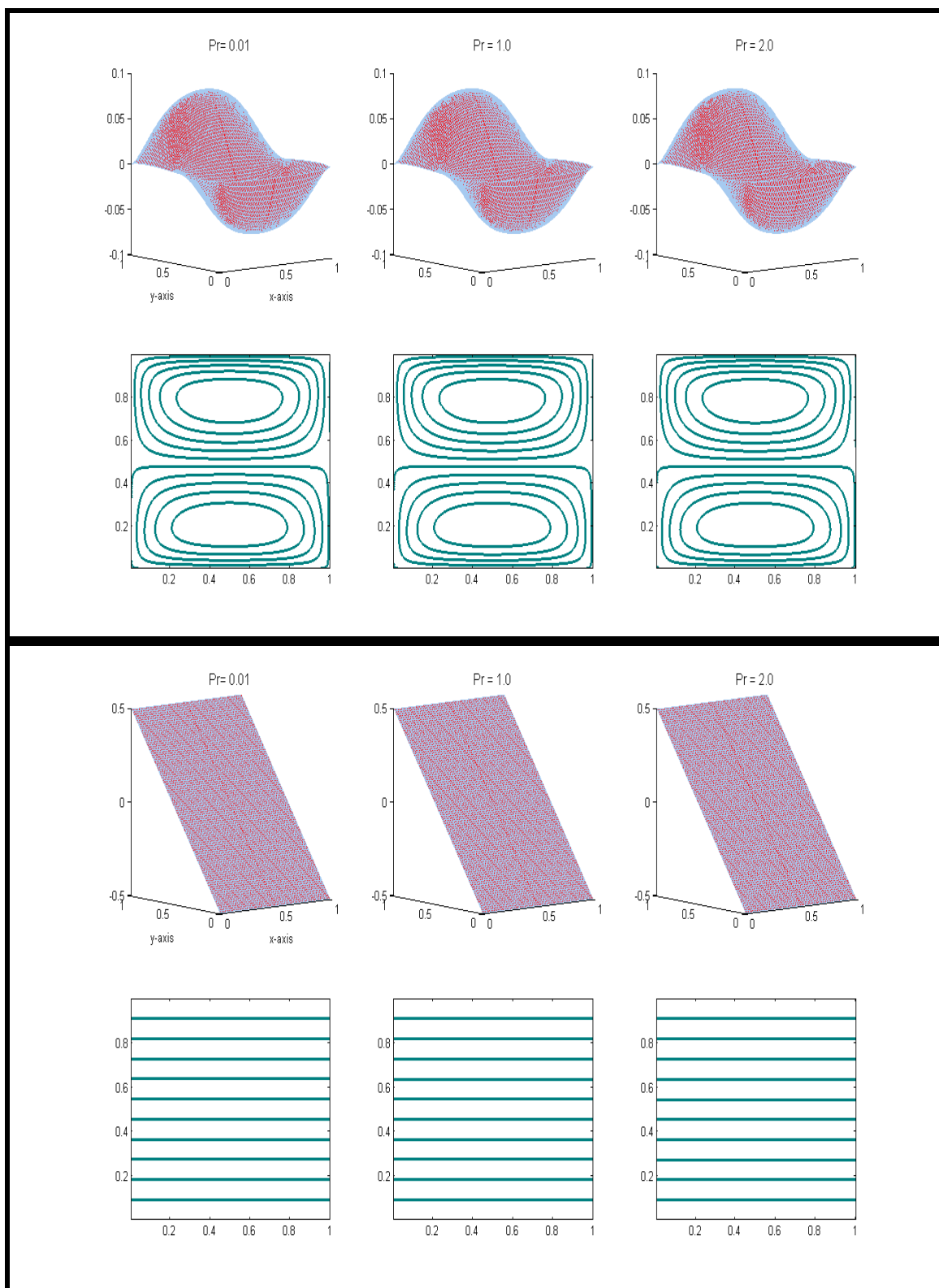


Figure 7a Contours of the velocity and temperature for distinct values of Prandtl number, Pr

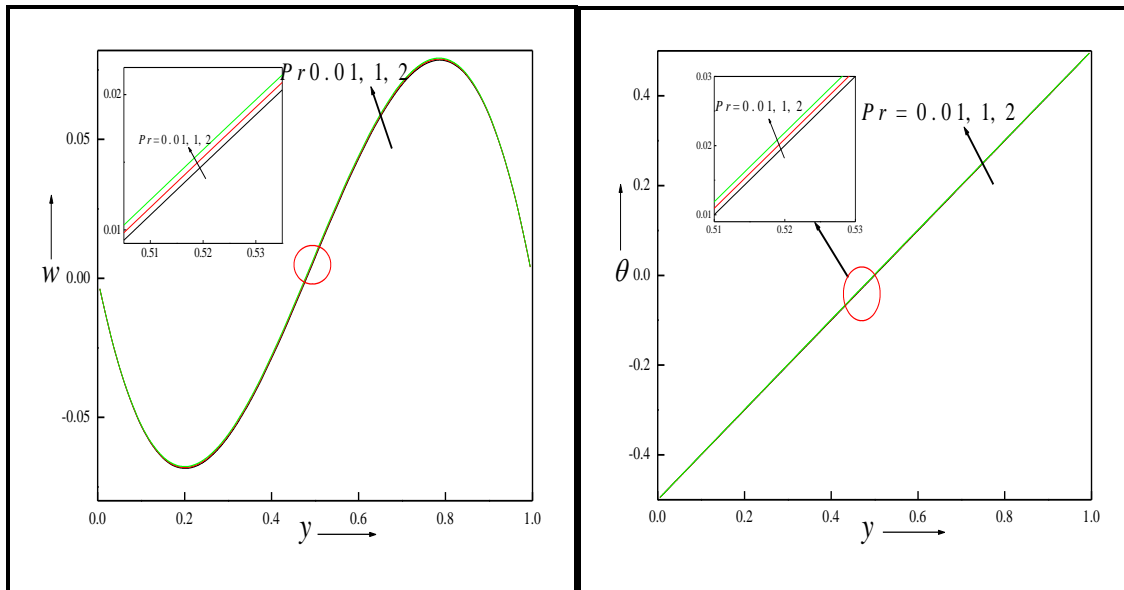
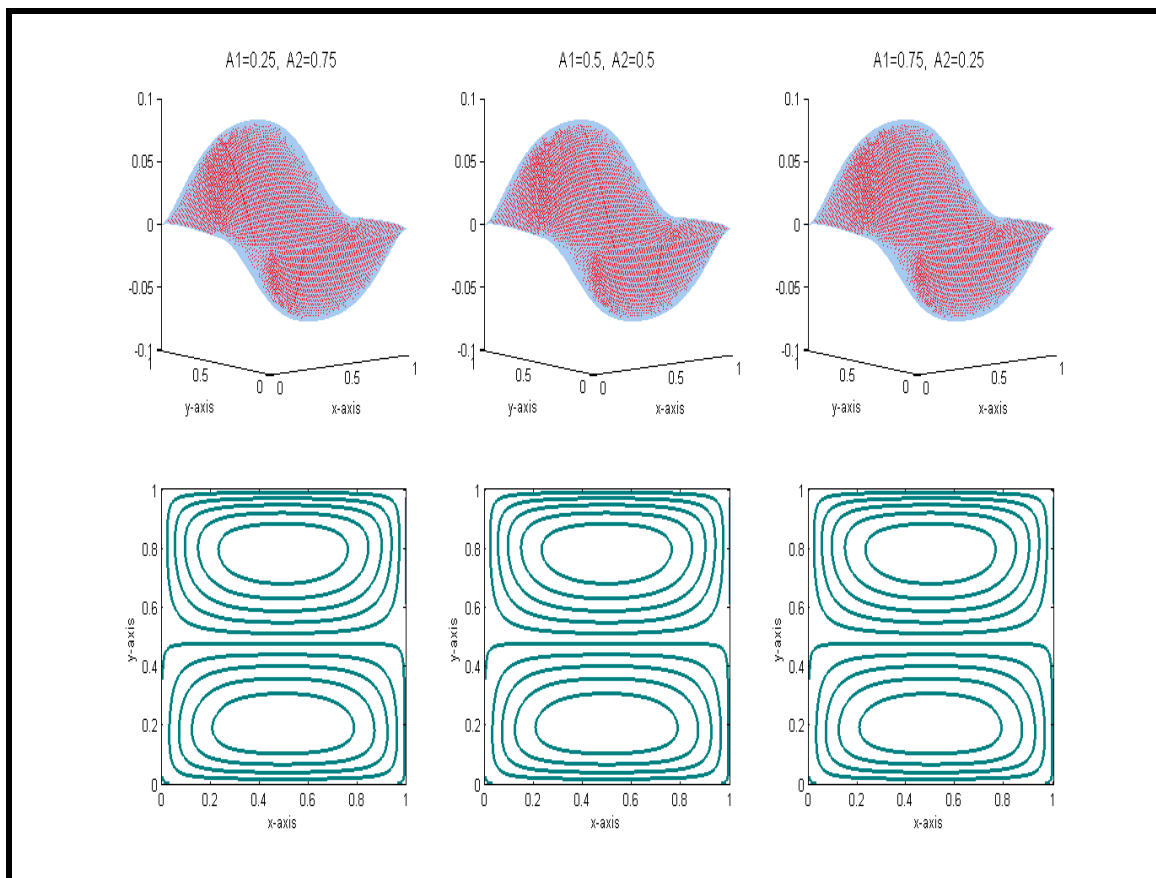


Figure 7b Portraits of velocity and temperature for different values of Prandtl number, Pr



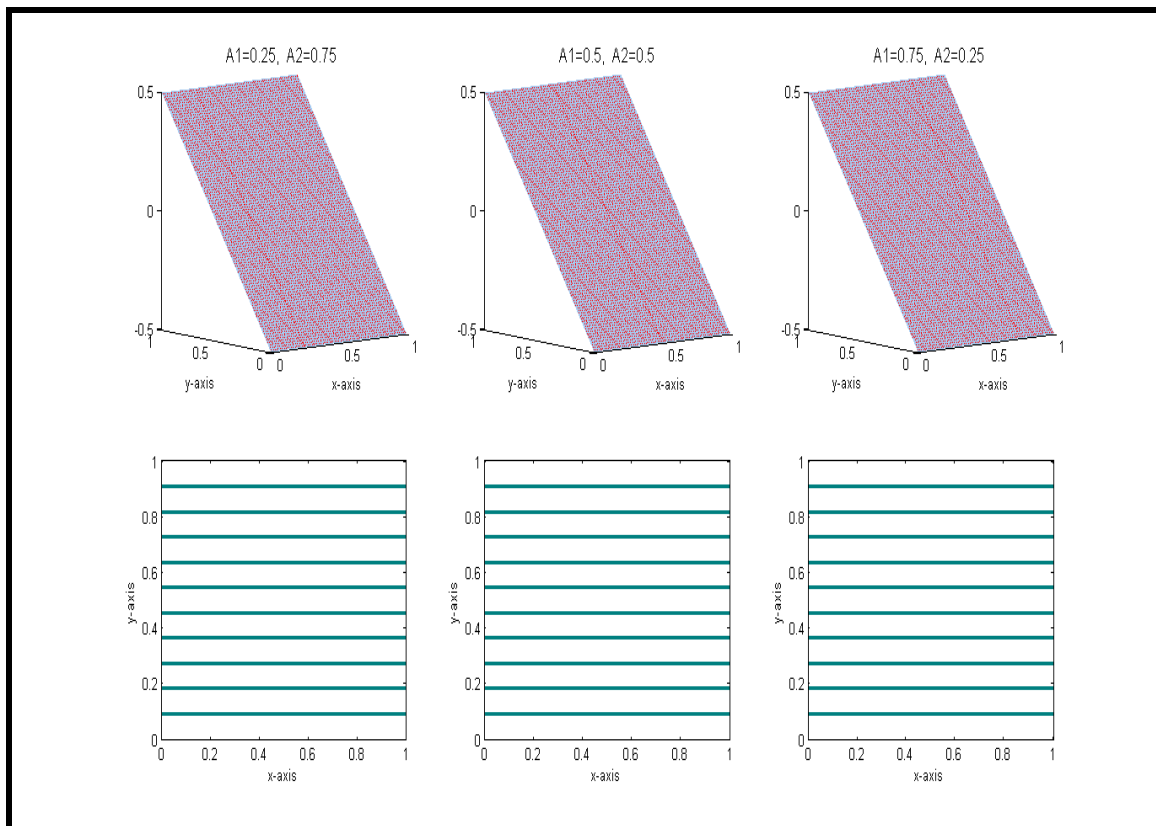


Figure 8a Contours of the velocity and temperature for distinct values of aspect ratio, A

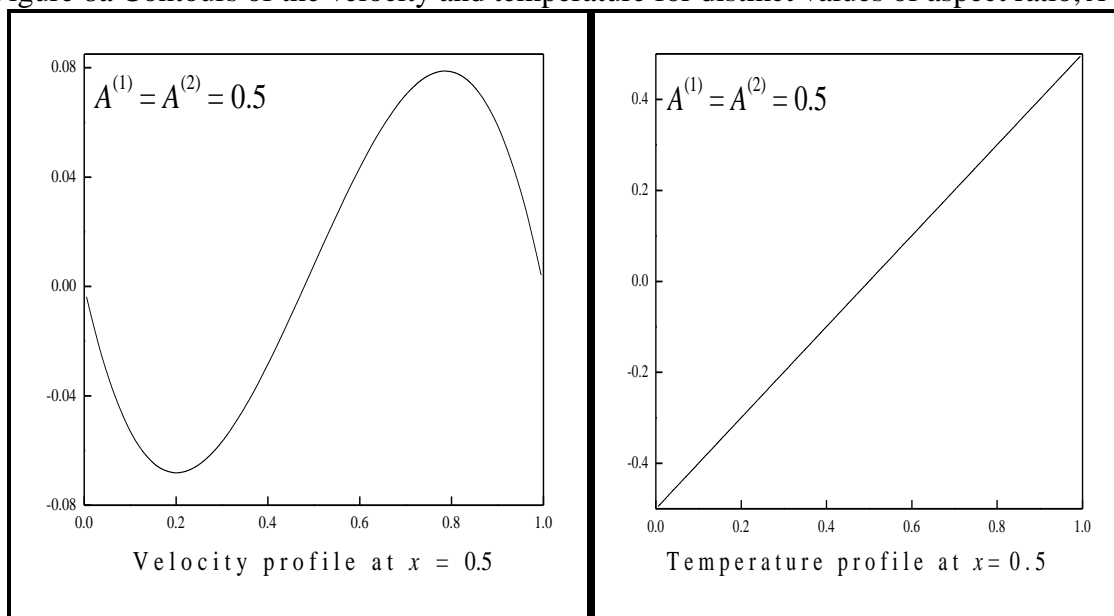


Figure 8b Portraits of velocity and temperature for different values of aspect ratio, A

	Region-1		Region-2	
	$Nu _{y=0}$	$Nu _{y=1}$	$Nu _{y=0}$	$Nu _{y=1}$
<i>Gr</i>				
5	1.00002647558	0.999934218804	1.00002647558	0.999934218804
10	1.00010830136	0.999813062987	1.00010830136	0.999813062987
20	1.00047480011	0.999367557524	1.00047480011	0.999367557524
50	1.00319174673	0.996398861098	1.00319174673	0.996398861098
100	1.01303336733	0.985919573505	1.01303336733	0.985919573505
α				
0.1	1.00842906339	0.990509837298	1.01798289150	0.979618331411
0.25	1.00546824270	0.993809055995	1.00837351924	0.990581253220
0.5	1.00414541714	0.995304806598	1.00503562913	0.994332403717
0.75	1.00355133762	0.995985064589	1.00383851681	0.995673426175
1.0	1.00319174673	0.996398861098	1.00319174673	0.996398861098
β				
0.1	1.00424898975	0.995259872848	1.02106876439	0.974952448685
0.25	1.00396933016	0.995568561323	1.00960809805	0.988844210899
0.5	1.00362420167	0.995938574299	1.00550814623	0.993702980600
0.75	1.00337715861	0.996201755690	1.00400575580	0.995457369157
1.0	1.00319174673	0.996398861098	1.00319174673	0.996398861098
<i>Ec</i>				
0.1	1.00319174673	0.996398861098	1.00319174673	0.996398861098
0.5	1.01582789841	0.981796831208	1.01582789841	0.981796831208
1.0	1.03134405437	0.963078469336	1.03134405437	0.963078469336
1.5	1.04657351828	0.943806662769	1.04657351828	0.943806662769
2.0	1.06154083944	0.923939250194	1.06154083944	0.923939250194
<i>Pr</i>				
0.01	1.00004569088	0.999948691037	1.00004569088	0.999948691037
0.5	1.00228118450	0.997429732829	1.00228118450	0.997429732829
1.0	1.00455555740	0.994849571201	1.00455555740	0.994849571201
1.5	1.00682319484	0.992259415933	1.00682319484	0.992259415933
2.0	1.00908417258	0.989659166577	1.00908417258	0.989659166577
$A^{(1)}, A^{(2)}$				
$A^{(1)} = 0.1$ $A^{(2)} = 0.9$	1.00263289473	0.997073628573	1.00325384136	0.996323886971
$A^{(1)} = 0.25$ $A^{(2)} = 0.75$	1.00288278000	0.996775638980	1.00329473564	0.996273268471
$A^{(1)} = 0.5$ $A^{(2)} = 0.5$	1.00319174673	0.996398861098	1.00319174673	0.996398861098
$A^{(1)} = 0.75$ $A^{(2)} = 0.25$	1.00329473564	0.996273268471	1.00288278000	0.996775638980

$A^{(1)} = 0.9$	1.00325384136	0.996323886971	1.00263289473	0.997073628573
$A^{(2)} = 0.1$				

Table 4: Values of average Nusselt number with $Gr = 50, \alpha = 1, \beta = 1, Ec = 0.1, Pr = 0.7, Re = 5.0, p = -0.1, A^{(1)} = 0.5, A^{(2)} = 0.5$

The graphs are plotted in three (3D), two (2D) and one (1D) dimensions to enhance understanding of the flow behavior. The one dimensional graphs are plotted for variations of y ranging from 0 to 1 for fixed value of x at 0.5. The graphs plotted in the top position are for 3D, in the bottom position are for 2D in the figure captions with the letter “a” and 1D with the figure captions using the letter “b”.

The effects of Grashof number Gr on the velocity and temperature fields are shown in Figs. 3a and 3b. Figure 3a (3D) shows that as the Grashof number increases flow increases in the upward direction. For small values of Gr the velocity contour is flat in the lower half region of the duct and steep in the upper half region of the duct. For large values of Gr the contours are steep in both the lower and upper region of the duct. From the 3-D graph one can also clearly identify the line of separation from region-1 and region-2. This is, due to the fact that, the value of the velocity in region-1 and region-2 is repeated at the interface as we have assumed the *continuity of velocity* at the interface. Therefore, in the numerical code at the interface, the value of the velocity appears twice and hence there is a clear boundary delineating region-1 and region-2. It is also evident from the 2D graph (Fig 3a) that the number of velocity contours are sparse in the lower half region and their density is increased as Gr increases. The effect of Grashof number Gr on the temperature is not significant. Here there is again a clear line in the 3D plot showing the separation of region-1 and region-2. This is again due to the assumption that *the temperature is continuous at the interface*.

The temperature contours (2D) are linear in nature for all values of Gr . To understand the effect of Grashof number at a fixed location (x), a 1D graph is drawn at $x = 0.5$ with y varying from 0 to 1 as shown in Fig. 3b. The velocity (values are negative) decreases as Gr increases in the downward direction in the region $0 \leq y \leq 0.5$ (lower zone 2). However, velocity (the values are positive) increases in the upward direction in the region $0.5 \leq y \leq 1.0$ (upper zone 1). Therefore, increasing buoyancy force exerts a

different impact in the two different zones. The temperature profiles are generally in close proximity for all values of Gr . However, temperature is enhanced at certain points in the enclosure with stronger buoyancy effect (higher Grashof number). An intensification of convective flow with Grashof number Gr is associated with a dominance of the buoyancy force relative to the viscous hydrodynamic force (all profiles correspond to $Gr > 1$) the modifications in temperature distributions concur with classical results. The effect of Grashof number on the flow is also similar to results observed by Malashetty *et al.* (2006) for the magneto-convective flow of immiscible fluids in a vertical channel.

The effect of viscosity ratio α on the velocity distribution is shown in Figs. 4a, b. The viscosity ratio α is defined as the ratio of viscosity of the fluid in region-1 to the fluid in region-2. The Fig. 3a shows that as α increases flow increases in region-2 ($0 \leq x \leq 0.5$). The value of $\alpha = 0.1$ implies that the viscosity of the fluid in region-2 is 10 times more than the viscosity of the fluid in region-1 ($0.5 \leq x \leq 1.0$). The 3D graphical plot for $\alpha = 0.1$ shows that the curvature of the flow in region-2 is flat, whereas for $\alpha = 0.5$, it is apparent that there is a curved topology to the flow in region-2 and the flow in region-1 and region-2 are asymmetric. For the value of $\alpha = 1.0$ (the viscosity of the fluids in region-1 and region-2 are equal) it is seen in Fig. 3a that the flow is symmetric in region-1 and region-2. Velocity magnitudes are known to be significantly lower for highly viscous fluids when compared with lower viscosity fluids. Therefore, as the viscosity of the fluid in region-2 decreases, there is an accompanying enhancement in velocity in region-2 whereas the velocity in region-1 remains unaltered since the viscosity ratio in region-1 is constrained as 1. Inspection of the plot also reveals the interfacial boundary line which distinguishes the flow in region-1 and region-2. The 2D graph also indicates that the contours are flat for values of α less than unity and are symmetric for $\alpha = 1.0$. The effect of α on the temperature is not substantial as seen in Fig. 3a. The temperature contours are linear in nature and the temperature field is only mildly distorted by the variations of the viscosity variation parameter α . Figure 3b implies that as α increases the velocity (for which values are negative) also increases in the upward direction in the region $0 \leq y \leq 0.5$ whereas it is depleted (velocity values of are positive)

in the region $0.5 \leq y \leq 1$. The 1D graph also clearly indicates that the temperature field is generally undisturbed with the variations of α .

The effect of the thermal conductivity ratio parameter β on the velocity and temperature profiles is displayed in Figs. 5a and 5b. The thermal conductivity is defined as the ratio of thermal conductivity of region-2 to the thermal conductivity of region-1. Figures 5a and 5b indicate that the velocity remains invariant to changes in β . Figure 5a also indicates that the flow is symmetric in both upper and lower duct regions and also the numbers of contours are equal for all values of β . The 1D graph also reflects that both the temperature profiles are basically unaltered for all values of the ratio of thermal conductivity parameter, β . Although thermal conductivity parameter β appears in the energy equation, it is observed from Figs. 3a and 3b that the temperature field is not modified prominently with this parameter. Increase in thermal conductivity parameter does not influence the flow since the top and bottom plates are insulated and hence there is no notable changes in the energy distribution and thereby no marked modification in velocity.

The effect of Eckert number on the flow field are displayed in Figs. 6a and 6b. From Fig. 6a one can infer that Eckert number does not induce any significant changes. The curvature (3D) and the number of contours (2D) are similar for all values of Eckert number except that one contour is concentrated in the upper cell for $Ec=1.0$ when compared with $Ec=0.1$ and the number of contours remain the same for $Ec=1.0$ and for $Ec=2.0$. However, Fig. 6b (1D) clearly visualize that as Eckert number increases there is slight increase in the velocity magnitudes i.e. the flow is weakly accelerated. The temperature profile generally is only marginally disturbed. However, where the temperature field is magnified, at a particular point, it is also further amplified as the Eckert number increases. Eckert number increases the dissipation effect (conversion of kinetic energy into thermal energy) and this assists the thermal buoyancy force in the momentum equation.

The effect of Prandtl number on the velocity and temperature fields is drawn in Figs. 7a and 7b. These figures reveal a similar influence to that which is caused by changing the Eckert number (Figs. 6a and 6b) on the velocity. With increasing Prandtl

number, the thermal conductivity of the fluid (s) is decreased, and temperatures are reduced. The effect of Eckert number and Prandtl number produce similar behaviors to those reported by Umavathi *et al.* (2010) for the Couette flow in a composite channel.

The effects of aspect ratios $A^{(1)}$ and $A^{(2)}$ on the velocity and temperature fields are shown in Figs. 8a and 8b. Since the aspect ratio $A^{(1)}$ is defined as the ratio of height of the fluid in region-1 to half of the width of the duct and the aspect ratio $A^{(2)}$ is defined as the height of the fluid in region-2 to half of the width of the duct, altering the values of the aspect ratios will result in *displacement of the interface*. For the value of $A^{(1)}=0.25$ and $A^{(2)}=0.75$ the interface is near the left wall of the duct, for the values of $A^{(1)}=0.5$ and $A^{(2)}=0.5$ the interface is at the centre of the duct and for the values of $A^{(1)}=0.75$ and $A^{(2)}=0.25$ the interface migrates to near the right wall of the duct. The position of the interface can be clearly seen in Fig. 8a (3D). Since the sum of the aspect ratios in region-1 and region-2 will be 1 for three different values of aspect ratios in region-1 and region-2, the velocity and temperature fields are undisturbed for the variations of the aspect ratios. Only the position of the interface is changed. The 1D graph (Fig. 8b) is drawn for only one set of values of aspect ratios $A^{(1)} = A^{(2)} = 0.5$. For other two combinations of the aspect ratios the profiles are not modified and hence not displayed.

Table-4 shows the values of Nusselt number for all the governing parameters at both left and right walls of the duct for region-1 and region-2. The values indicate that as the Grashof number Gr , Eckert number Ec , Prandtl number Pr and aspect ratio $A^{(1)}$ increases ($A^{(2)}$ decreases), there is an escalation in the Nusselt number at the left wall whereas there is a suppression in Nusselt number at the right wall in both regions whereas the contrary effect is observed for increasing values of viscosity ratio α and thermal conductivity ratio β . Furthermore, it is noteworthy that the values of Nusselt number remain the same in region-1 and region-2 with changing the Grashof number Gr , Eckert number Ec and Prandtl number Pr whereas the Nusselt number magnitudes are different in region-1 and region-2 with changing the viscosity ratio α , conductivity ratio β and aspect ratios $A^{(1)}$, $A^{(2)}$. Table-4 clearly indicates that there is not much variation

in the values of Nusselt number with Eckert number which has only a slight effect on the flow. The dissipation is swamped by buoyancy effects (Grashof number) which are dominant in this regime. It can also be stated that the Nusselt number does not vary significantly with any of the governing parameters as there is no notable change in the energy at the boundaries (plates). However, the rank of impacting parameters in Nusselt number, from highest to lowest, can be listed as respectively, aspect ratio, Eckert number, thermal conductivity ratio, viscosity ratio, Grashof number and Prandtl number. In terms of percentages, $Nu|_{y=0}$ changes are 19.3334, 19.9350, 19.9423, 19.9965, 20.1926% in correspondence with a change in Grashof number from 5, 10, 20, 50, to 100 respectively. For aspect ratio (the highest ranking) percentage change in Nusselt number is 19.9916 $(A^{(1)} = 0.1, A^{(2)} = 0.9)$, 19.9966 $(A^{(1)} = 0.25, A^{(2)} = 0.75)$, 20.0028 $(A^{(1)} = 0.5, A^{(2)} = 0.5)$, 20.0048 $(A^{(1)} = 0.75, A^{(2)} = 0.25)$, 20.0040 $(A^{(1)} = 0.9, A^{(2)} = 0.1)$. The percentage change in Nusselt number (the lowest ranking) is 19.9102, 19.9547, 19.9999, 20.0451, 20.0901% for values of Prandtl number of 0.01, 0.5, 1.0, 1.5, 2 respectively. These variations show that there is a non-trivial sensitivity of the wall heat transfer rate with different control parameters in the model.

5. CONCLUSIONS

The steady laminar fully developed natural thermal convection flow in two immiscible viscous incompressible fluids in a vertical rectangular duct has been investigated. The dimensionless momentum and energy equations governing the flow in the two regions have been solved numerically using a finite difference method and the following conclusions are drawn:

1. The validity of the solutions is confirmed with a grid (mesh) independence study. The computational solutions obtained have also been compared with the benchmark solutions of de Vahl Davis and Jones (1983), Sanchez *et al.* (2004) Kaminski and Prakash (1986) for the one-fluid model and with Haken *et al.* (2009) and Moshkin (2002) for the two-fluid model and experimental results.

2. The effects of the emerging pertinent thermophysical and hydrodynamic parameters on the momentum and thermal characteristics have been visualized graphically and interpreted. It has been found that as Grashof number, Eckert number and Prandtl number are increased there is a substantial enhancement in the velocity and a less prominent influence on temperature distributions.
3. As the viscosity ratio parameter increases flow acceleration is induced in the upper half region of the duct and deceleration is caused in the lower half of the duct.
4. The viscosity ratio and thermal conductivity ratio parameters do not exhibit a significant impact on the flow and heat transfer.
5. Assigning different values of aspect ratios in the two regions ($A^{(1)}$ and $A^{(2)}$) generates a noticeable movement of the interface whereas the magnitude of the flow and heat transfer is largely unaltered.
6. As the Grashof number, Eckert number, Prandtl number and aspect ratio $A^{(1)}$ increase (i.e. with simultaneous decrease in $A^{(2)}$) the Nusselt number increases at the left wall and decreases at the right wall in both the regions. However, the reverse effect is observed for increasing values of viscosity ratio and thermal conductivity ratio.
7. The present numerical code provides stable and accurate solutions for two-fluid convection heat transfer flows and may be applied in future to extend the current study to consider *non-Newtonian* liquids.

ACKNOWLEDGEMENTS

The authors appreciate the detailed comments of the reviewers and editor which have improved the article.

REFERENCES

- Abu-Nada, E., 2015. Dissipative particle dynamics simulation of natural convection using variable thermal properties, *Int. Comm. Heat and Mass Transfer*, 69, 84-93.
- Alazmi, B., Vafai, K., 2001. Analysis of fluid flow and heat transfer interfacial conditions between a porous medium and a fluid layer. *Int. J. Heat Mass Transfer*, 44, 1735-1749.

- Bég, O. Anwar, N. Ali, A. Zaman, Eemaan T. A. Bég and Ayesha Sohail, 2016. Computational modelling of heat transfer in annular porous medium solar energy absorber with a P1-radiative differential approximation, *J. Taiwan Inst. Chemical Eng.*, 66, 258-268.
- Bethancourt, A.M.L., Hashiguchi, M., Kuwahara, K., Hyun, J.M., 1999. Natural convection of two-layer fluid in a side-heated cavity. *Int. J. Heat and Mass Transfer*, 42, 2427-2437.
- Bhargava, S. Sharma, P. Bhargava, O. Anwar Bég and A. Kadir, 2017. Finite element simulation of nonlinear convective heat and mass transfer in a micropolar fluid-filled enclosure with Rayleigh number effects, *Int. J. Applied Computational Mathematics*, 3 (2), 1347–1379.
- Braga, J.E. and de Lomos, M.J.S., 2005. Heat transfer in enclosures having a fixed amount of solid material simulated with heterogeneous and homogeneous models. *Int. J. Heat and Mass Transfer* 48, 4748-4765.
- Chamkha, A. J., 1994, Unsteady flow of dusty conducting fluid through a pipe, *Mechanics Research Communications*, 21, 281-288.
- Chamkha, A. J., Hydromagnetic two-phase flow in a channel, 1995, *Int.J.Engng.Sci*, 33, 437-446.
- Chamkha, A. J., 1997, Non-Darcy fully developed mixed convection in a porous medium channel with heat generation/absorption and hydromagnetic effects, *Numerical Heat Transfer, Part A*, 32, 653-675.
- Chamkha, A. J., 2000, Unsteady laminar hydromagnetic fluid-particle flow and heat transfer in channels and circular pipes, *Int.J.Heat and Fluid Flow*, 21, 740-746.
- Chamkha, A. J., 2002, On laminar hydromagnetic mixed convection flow in a vertical channel with symmetric and asymmetric wall heating conditions, *IJHMT*, 45, 2509-2525.
- Chamkha, A. J., 2001, Unsteady laminar hydromagnetic flow and heat transfer in porous channels with temperature-dependent properties, *Int.J. Numerical Methods for Heat and Fluid Flow*, 11, 430-448.
- Chamkha, A. J., Grosan, T. and Pop, I., 2002, Fully developed free convection of a micropolar fluid in a vertical channel, *Int. Commu. Heat Mass Transfer*, 29, 1119-1127.

- Chamkha, A. J., and Al-Subaie, M.A., 2009, Hydromagnetic buoyancy-induced flow of a particulate suspension through a vertical pipe with heat generation/absorption effects, *Turkish J. Eng. Env. Sci.*, 33, 127-134.
- Chamkha, A. J. and Salva Parvin, 2014, An analysis on free convection flow, heat transfer and entropy generation in an odd-shaped cavity filled with nanofluid, *Int. Comm. in Heat and Mass Transfer*, 54, 8-17.
- Chamkha, A. J., Maysam Molana, Ali Rahnama and Farid Ghadami, 2018, On the nanofluid applications in microchannels: A comprehensive review, *Powder Technology* (Accepted), doi:10.1016/j.powtec.2018.03.044.
- De Vahl Davis, G., 1983. Natural convection of air in a square cavity. *Int. J. Num. Meth. Fluids*, 3, 249-264.
- Dobretsov, N.L., Kyrdyashkin, A.G., 1993. Experimental modeling of two-layer mantle convection. *Ofoliti*, 18 (1), 61–81.
- B. Gebhart *et al.*, *Buoyancy-induced Flows and Transport*, Hemisphere, Washington, USA (1988).
- Hall, J.D., Bejan, A., Chaddock, J.B., 1988. Transient natural convection in a rectangular enclosure with one heated side wall. *Int. J. Heat Fluid Flow* 9, 396-404.
- Kaminski, D.A., Prakash, C., 1986. Conjugate natural convection in a square enclosure: effect of conduction in one of the vertical walls. *Int. J. Heat Mass Transfer* 29, 1979-1988.
- Kays, W.M. and Crawford, M.E. *Convective Heat and Mass Transfer*. 3rd Edition, McGraw Hill, New York, USA (1993).
- Kefayati, G.H.R., S.F. Hosseinizadeh, M. Gorji, H. Sajjadi, 2011. Lattice Boltzmann simulation of natural convection in tall enclosures using water/SiO₂ nanofluid, *Int. Comm. Heat and Mass Transfer*, 38, 6, 798-805.
- Keimanesh, M., Reshidi, M.M., Chamkha, A. J. and Jafari, R., 2011, Study of third grade non-Newtonian fluid flow between two parallel plates using the multi-step differential transformed method, *Computers and Mathematics*, 62, 2871-2891.
- Kim, N.H., Tae-Yong Sin, 2006. Two-phase flow distribution of air-water annular flow in a parallel flow heat exchanger. *Int. J. Multiphase Flow* 32, 1340-1353.

- Kimura, S., Bejan, A., 1984. The boundary layer natural convection regime in a rectangular cavity. *ASME J. Heat Transfer* 106, 98-103.
- Kimura, T., Heya, N., Takeuchi, M., Isomi, H., 1986. Natural convection heat transfer phenomena in an enclosure filled with two stratified fluid, *Japan Soc. Mech. Eng. (B)* 52, 617-625.
- Kuharat, S., O. Anwar Bég, Ali Kadir, B. Vasu, Tasveer A. Bég and W.S. Jouri, 2019. Computation of gold-water nanofluid natural convection in a three-dimensional tilted prismatic solar enclosure with aspect ratio and volume fraction effects, *Nanoscience and Technology- An International Journal*. **In press**
- Kuznetsov, A.V., 2000, Analytical studies of forced convection in partly porous configurations, In: *Vafai K. (Eds.). Handbook of Porous Media*, Marcel Dekker, New York, USA, 269-312.
- Longlois, W.E., 1985. Buoyancy-driven flows in crystal-growth melts. *Ann. Rev. Fluid Mech.* 17, 191-215.
- Lohrasbi, J., Sahai, V., 1998. Magnetohydrodynamic heat transfer in two phase flow between parallel plates, *Appl. Sci. Res.* 45, 53-66.
- Malashetty, M.S., Umavathi, J.C., 1997. Two phase magnetohydrodynamic flow and heat transfer in an inclined channel. *Int. J. Multiphase Flow*, 23, 545-560.
- Malashetty, M.S., Umavathi, J.C., Prathap Kumar, J., 2001. Convective flow and heat transfer in a composite porous medium. *J. Porous Media* 4, 15-22.
- Malashetty, M.S., Umavathi, J.C., Prathap Kumar, J., 2006. Magneto convection of two immiscible fluids in a vertical enclosure. *Heat Mass Transfer*, 42, 977-993.
- Mayer, H.I., Garder, A.O., 1954. Mechanics of two immiscible fluids in porous media *J. Applied Physics* 25, 1400-1406.
- Moosavi, L., N. M. Norafida, G. M. A. Ismail, 2014. Thermal performance of atria: An overview of natural ventilation effective designs, *Renewable and Sustainable Energy Reviews*, 34, 654-670.
- N. P. Moshkin, 2002. Numerical model to study natural convection in a rectangular enclosure filled with two immiscible fluids. *Int. J. Heat and Fluid Flow* 23, 373-379.

- Mehryan, S.A.M., Kashkooli, F.M., Ghalambaz, M., and Chamkha, A. J., 2017, Free convection of hybrid $Al_2O_3 - Cu$ water nanofluid in a differentially heated porous cavity, *Advanced Powder Technology*, 28, 2295-2305.
- Mohebbi, R., Izadi, M., and Chamkha, A. J., 2017, Heat source location and natural convection in a C-shaped enclosure saturated by a nanofluid, *Physics of Fluids*, 29, 1220091-12200912.
- Nield D.A., Kuznetsov, A.V., 2000, Effect of heterogeneity in forced convection in a porous medium: parallel plate channel or circular duct. *Int. J. Heat Mass Transfer*, 43, 4119-4134.
- Ostrach, S., 1982. Low-gravity fluid flows. *Ann. Rev. Fluid Mech.* 14, 313-345.
- Oztop, H.F., Yasin Varol, Ahmet Koca, 2009. Natural convection in a vertically divided square enclosure by a solid partition into air and water regions. *Int. J. Heat and Mass Transfer*, 52, 5909-5921.
- Packham, B.A., Shail, R., 1971. Stratified laminar flow of two immiscible fluids. *Proc. Camb. Phil. Soc.* 69, 443-448.
- Pepper, D. and Wang, X., 2008. An hp-adaptive finite element model for heat transfer within partitioned enclosures, *Int. J. Numerical Methods for Heat & Fluid Flow*, 18, 1000-1014.
- Pop, I.I. and Ingham, D.B., Eds., *Convective Heat Transfer: Mathematical and Computational Modelling of Viscous Fluids and Porous Media*. Elsevier Science & Technology Books, The Netherlands (2001).
- Prakash, A., Koster, J.N., 1996. Steady Rayleigh-Bernard convection in a two-layer system of immiscible liquids. *ASME J Heat Transfer*, 118, 366-373.
- Prakash, A., Koster, J.N., 1997. Steady natural convection in a two-layer system of immiscible liquids. *Int. J. Heat Mass Transfer* 40, 2799-2812.
- Prathap Kumar, J., Umavathi, J.C., Chamkha, A.J. and I. Pop, 2010, Fully developed free-convective flow of micropolar and viscous fluids in a vertical channel, *Applied Mathematical Modelling*, 34, 1175-1186.
- RamReddy, Ch., Murhty, P.V.S.N., Chamkha, A. J., and Rashad, A.M., 2013, Soret effect on mixed convection flow in a nanofluid under convective boundary condition, *International Journal of Heat and Mass Transfer*, 64, 384-392.

- Ravnik, J., L. Škerget and Z. Žunič, 2008. Velocity–vorticity formulation for 3D natural convection in an inclined enclosure by BEM, *International Journal of Heat and Mass Transfer*, 51, 4517-4527.
- W. Rohsenow, J. Hartnett and Y. Cho, *Handbook of Heat Transfer*, 3rd Edition, McGraw Hill, New York, USA (1998).
- Rudraiah, N., Barron, R.M., Venkatchallappa, M., Subbaraya, C.K., 1995. Effect of magnetic field on free convection in a rectangular enclosure. *Int. J. Eng. Sci.*, 33, 1075-1084.
- Sanchez, F, Solorio, F., Avila, R., 2004. Conjugate natural convection in a square cavity heated from below, in: *Proceedings of IMECE04, ASME Int. Mech. Eng. Congress and exposition, Anaheim, California, USA*, 1-10.
- Schwabe, D., 1986. Surface-tension-driven flow in crystal growth metals. *Crystal*, 11, 848-852.
- Shail, R., 1973. On laminar two-phase flow in magneto hydrodynamics. *Int. J. Eng. Sci.* 11, 1103-1108.
- Sparrow, E.M., Azevedo, L.F.A., Prata, A.T., 1986. Two-fluid and single-fluid natural convection heat transfer in an enclosure, *ASME J. Heat Transfer* 108, 848-852.
- Umavathi, J.C., Chamkha, A.J., Abdul Mateen, Al-Mudhaf, A., 2005. Unsteady two-fluid flow and heat transfer in a horizontal channel. *Heat Mass Transfer* 42, 81-90.
- Umavathi, J.C., Abdul Mateen, Chamkha, A.J., Al-Mudhaf, A., 2006. Oscillatory Hartman two-fluid flow and heat transfer in a horizontal channel. *Int. J. Appl. Mech. Eng.* 11, 155-178.
- Umavathi, J.C., Manjula, M.H., Pop, I., Liu, I.C., 2007. Flow and heat transfer of couple stress and viscous fluid in a vertical channel. *Int. J. Appl. Mech. Eng.* 12, 537-555.
- Umavathi, J.C., Chamkha, Ali J., Sridhar, K.S.R., 2010. Generalised plain Couette flow and heat transfer in a composite channel. *Transport Porous Media* 85, 157-169.
- Umavathi, J.C., Prathap Kumar, J., Chamkha, A. J., and Pop, I., 2005, Mixed convection in a vertical porous channel, *TIPM*, 61, 315-335.
- Umavathi, J.C., Chamkha, A. J., Mateen, A., and Al-Mudhaf, A., 2009, Unsteady oscillatory flow and heat transfer in a horizontal composite porous medium channel, *Nonlinear Analysis: Modeling and Control*, 14, 397-415.

- Vafai, K., Kim, S.J., 1995. On the limitations of the Brinkman-Forchheimer-extended Darcy equation. *Int. J. Heat and Fluid Flow* 16, 11-15.
- Vafai, K., Kim, S.J., 1990, Fluid mechanics of the interface region between a porous Medium and a fluid layer: an exact solution. *Int. J. Heat Fluid Flow* 11, 254-256.
- Vahl Davis, G., 1968. Laminar natural convection in an enclosed rectangular cavity. *Int. J. Heat Mass Transfer*, 11, 167-1693.
- K. Venkatadri, S. A. Gaffar, M. S. Reddy, V. R. Prasad, B. M. H. Khan and O. Anwar Bég, 2020. Melting heat transfer analysis on magnetohydrodynamics buoyancy convection in an enclosure: a numerical study, *J. Applied and Computational Mechanics* 6(1) 52-62.
- Zehba, A.M.A. and A. S. Raizah, 2016. Double-diffusive natural convection in an enclosure filled with nanofluid using ISPH method, *Alexandria Engineering Journal*, 55, 3037-3052.
- Zukoski, E.E., T. Kubota, and B. Cetegen, 1980. Entrainment in fire plumes, *Fire Safety Journal*, 3, 107–121.